Chapter 16
Diffuse Rings

M. Horányi, J.A. Burns, M.M. Hedman, G.H. Jones, and S. Kempf

Abstract In order to give context to *Cassini*'s findings about Saturn's diffuse rings, this chapter first recalls the *Voyager* and telescopic observations prior to 2004. *Cassini* has investigated these faint rings composed of small particles with remote sensing (visual and infrared imaging) and in-situ detectors (charged-particle and dust detectors), for the first time allowing results obtained by the different techniques to be compared. Generally the agreement is good. The description of the observations are organized by increasing distance from Saturn, and includes (a) the faint rings in and around the main rings; (b) spokes in the B-ring; (c) the narrow outer faint rings; (d) the E-ring with emphasis on its connection to Enceladus's geysers; and (e) the Saturnian dust streams. These discussions also summarize relevant models that have been proposed to explain the behavior of charged dust grains. Except for the spokes and much of the E ring, the particles in these rings are collisional debris. Saturn's D ring has changed significantly since Voyager; part of it seems to be inclined and winding up while another portion (and the Roche Division) has periodic structures that are forced by Saturn's magnetic field. The faint rings in ring gaps are also time-variable and some have Sun-aligned elliptical orbits. The reappearance of the enigmatic spokes should allow several recent theories to be tested. Rings and arcs have been discovered to accompany *Cassini*-found small moons that are trapped in satellite resonances. The realization that Enceladus feeds the E ring and the opportunity to make in-situ measurements, including the electric charge and composition of grains, has made this a rich topic. The dust streams are composed of nanoscale particles moving at speeds of many tens to hundreds of km s^{-1}; they likely originate in the outer reaches of the E ring.

M. Horányi (✉)
Laboratory for Atmospheric and Space Physics, and Department of Physics, University of Colorado, Boulder, CO 80309–0392, USA

J.A. Burns and M.M. Hedman
Department of Astronomy, Cornell University, Ithaca, NY 14853, USA

J.A. Burns is also at the Department of Theoretical and Applied Mechanics, Cornell University, Ithaca, NY 14853, USA

G.H. Jones
Mullard Space Science Laboratory, University College London, Holmbury St. Mary, Dorking, Surrey, RH5 6NT, UK
and
The Centre for Planetary Sciences at UCL/Birkbeck, Gower St., London WC1E 6NT, UK

S. Kempf
Max Planck Institute for Nuclear Physics, Saupfercheckweg 1, Heidelberg, 69117, Germany

16.1 Introduction

In addition to its majestic main rings, Saturn also possesses a suite of diffuse, low optical depth rings composed primarily of particles less than 100 microns in radius. Interparticle collisions are rare in these tenuous rings, and the small sizes of the particles make them sensitive to non-gravitational forces, so the dynamics of these diffuse rings are qualitatively different from those in the main rings. Furthermore, while the main rings of Saturn can be studied only by remote sensing, the diffuse rings offer a unique opportunity to combine both remote-sensing and in-situ observations. The combination of these sets of data permits us to learn about the effects of phenomena such as radiation pressure, magnetospheric interactions, and plasma drag.

Figure 16.1 shows the entire ring system as seen by *Cassini* when it flew through Saturn's shadow on September 15, 2006. In this particular viewing geometry, small particles scatter light very efficiently, so all of the dusty rings can be detected with a relatively high signal-to-noise ratio. The D ring, the innermost component of Saturn's ring system, can be seen just interior to the main rings. Within the main rings, several narrow dusty ringlets can be detected, and even a few spokes are visible hovering over the B ring. Beyond the F ring, which is the brightest ring of all in this image, there is a series of narrow dusty rings, the brightest of which is the G ring. Furthest out, the extensive E ring fills the entire space between the orbits of Mimas and Rhea.

After summarizing the ground-based and Hubble Space Telescope (HST) observations of Saturn's diffuse rings since

M.K. Dougherty et al. (eds.), *Saturn from Cassini-Huygens*,
DOI 10.1007/978-1-4020-9217-6_16,

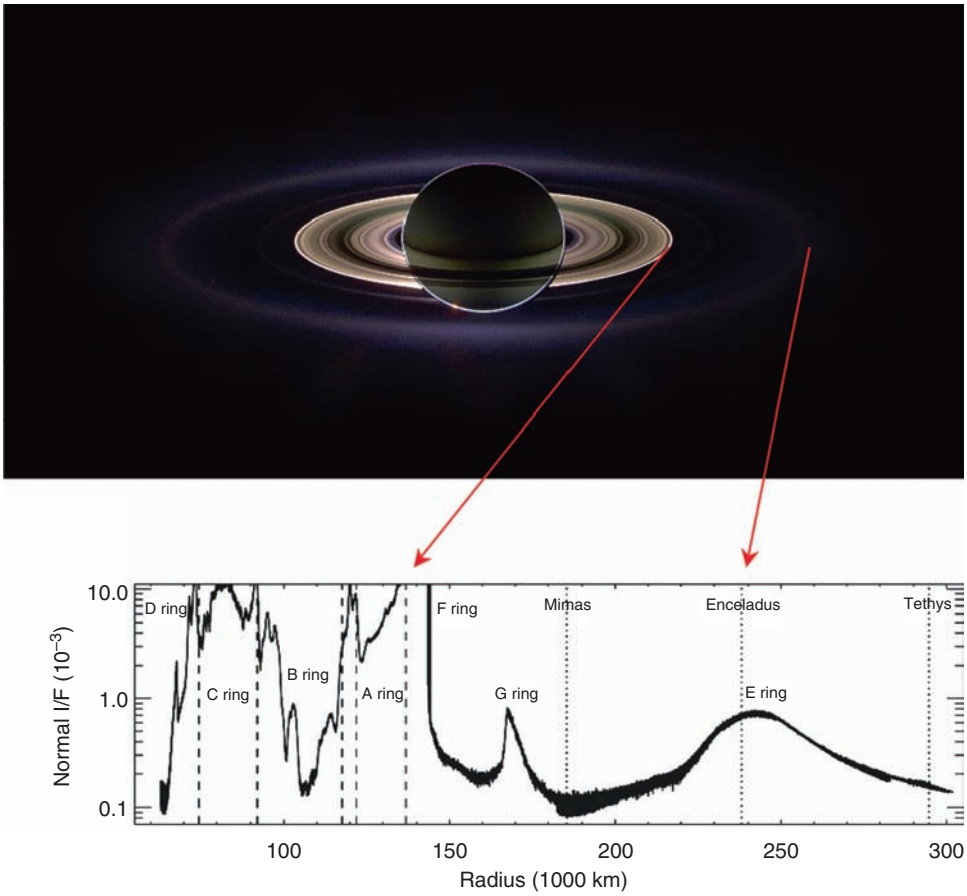

Fig. 16.1 *Top*: A mosaic of images taken on September 15, 2006 while *Cassini* was in the shadow of Saturn (image # PIA08329). The red, green and blue colors in this image are derived from images taken in the IR3, clear and VIO filters. In this geometry the small particles that mostly comprise the diffuse rings scatter light very efficiently, so these normally faint rings appear especially bright. *Bottom*: the brightness of the rings as a function of radial distance from Saturn for a constant phase angle of 178.5° as observed through the camera's clear filter (central wavelength of 635 nm). Brightness is plotted in terms of a quantity called normal I/F, which is proportional to the fraction of the incoming solar radiation scattered into the camera by the material

Voyager, we describe new *Cassini* results for the diffuse rings. We also mention the dust streams of nanoparticles because they are subject to non-gravitational forces and because they likely originate in the outer reaches of Saturn's E ring. Table 16.1 provides the locations and properties of the diffuse rings discussed in this chapter. Note that the F ring, while also composed predominantly of small particles and in most places having low optical depth, is not discussed here, but is instead described in Chapter 13.

16.2 Pre-*Cassini* Observations

Before *Cassini*, the state of knowledge about the properties of Saturn's faint rings and the processes responsible for shaping them were mainly based on *Voyager* observations, which have been discussed in various reviews (Burns et al. 1984, Grün et al. 1984, Mendis et al. 1984, Burns et al. 2001, Horányi et al. 2004). Detailed studies of the D, G and E rings (Showalter et al. 1991, Showalter and Cuzzi 1993, Showalter 1996) and the spokes in the B ring (Porco 1983) that review Voyager data are also available, and therefore do not need to be repeated here.

After the *Voyager* flybys, the next valuable opportunity to observe Saturn's faint rings came in 1995–1996, when Earth passed three times through the planet's ring plane. At this time, the line-of-sight optical depth through the faint rings was greatly enhanced, while the glare from the main rings was reduced. The G and E rings were each observed with HST as well as with large ground-based telescopes like Keck. These observations confirmed that the core of the E ring has a strong blue spectral slope in backscattered light, while the G ring has a slightly red slope between the visible and the near infrared (Nicholson et al. 1996, de Pater et al. 1996, Bauer et al. 1997, de Pater et al. 2004). These color differences provided evidence that these two rings had very different particle size distributions. The G ring's red

Table 16.1 Properties of Saturn's Diffuse Rings

Main ring	Diffuse ring	Radial location	Optical depth	Source
	D Ring Inner Edge	65,000km		Hedman et al. (2007a)
	D68	67,600 km	$\sim 10^{-4}$ (inside 73,000 km)	
	D72	71,600 km	$\sim 10^{-3}$ (outside 73,000 km)	
	D73	73,300 km		
	D Ring Outer Edge	74,500 km		
74,500 km				
C	Dusty Ringlet in the Maxwell Gap	87,420 km	10^{-4}	Porco et al. (2005)[a]
91,980 km				
B	Spokes	100,000–117,500 km	$10^{-2} - 10^{-1}$	Smith et al. (1981, 1982)
117,500 km				
Cassini	Dusty Ringlet in the Huygens Gap	117,490 km	10^{-4}	Porco et al. (2005)[a]
Division	Charming Ringlet in the Laplace Gap	119,940 km	10^{-3}	Porco et al. (2006)[b]
122,100 km				
A	Inner Encke Gap Ringlet	133,490 km	10^{-3} (up to 0.1 in clumps)	Porco et al. (2005)[a]
	Central Encke Gap Ringlet	133,590 km	10^{-3} (up to 0.1 in clumps)	
	Fourth Encke Gap Ringlet	133,660 km	$\sim 10^{-4}$	
	Outer Encke Gap Ringlet	133,720 km	10^{-3} (up to 0.1 in clumps)	
136,800 km				
	Roche Division	136,800 km–139,500 km	$\sim 10^{-4}$	Burns et al. (2002), Porco et al. (2005)
	F ring Core	140,200 km	0.2	Bosh et al. (2002)
	F ring Spiral	139,500 km–141,000 km	$\sim 10^{-2}$	Charnoz et al. (2005), Murray et al. (2008)
	Janus/Epimetheus Ring	151,450 km	$\sim 10^{-7}$	Porco et al. (2006)[c]
	G Ring	165,000 km–175,000 km	10^{-6}	Hedman et al. (2007b)
	G Ring Arc	167,500 km	10^{-5}	
	Methone Ring Arc	194,230 km	$\sim 10^{-7}$	Hedman et al. (2009a)[c]
	Anthe Ring Arc	197,650 km	$\sim 10^{-7}$	Hedman et al. (2009a)[c]
	Pallene Ring	212,280 km	$\sim 10^{-7}$	Hedman et al. (2009a)[c]
	E ring	180,000 km–700,000 km	10^{-5} (Peak)	Showalter et al. (1991)

[a] Optical depth assuming rings primarily dust (τ_{min} in Table 3).
[b] Optical depth based of VIMS measurements.
[c] Optical depth estimates based of brightness relative to G ring.

color, similar to those of other dusty rings, is consistent with broad size distributions like power laws and physical models of collisional debris (Showalter and Cuzzi 1993, Throop and Esposito 1998). By contrast, the blue color of the E ring suggests a very steep or narrow size distribution (Showalter et al. 1991), indicating that the particles in the E ring are generated or dispersed by different mechanisms than those active in the G ring.

Observations during this ring-plane crossing also provided improved measurements of the radial and vertical structure of these rings. The G ring was found to have a relatively sharp inner edge and a more diffuse outer boundary (Lissauer and French 2000), in agreement with *Voyager* measurements (Showalter et al. 1991), although the implications of this shape were not yet understood. The E ring (Fig. 16.2) was confirmed to have an asymmetric radial profile that peaked outside Enceladus's orbit (de Pater et al. 2004). Ground-based observations were also able to resolve the vertical structure of the E ring, showing it had a minimum vertical thickness at Enceladus's orbit and became progressively wider with increasing distance from that moon (Nicholson et al. 1996, de Pater et al. 2004). Finally, observers (Roddier et al. 1998) saw what might have been a temporary arc of material in the E ring close to the orbit of Enceladus. All this reinforced an early model that the E ring was closely linked to Enceladus, an idea that would be amply corroborated by *Cassini*.

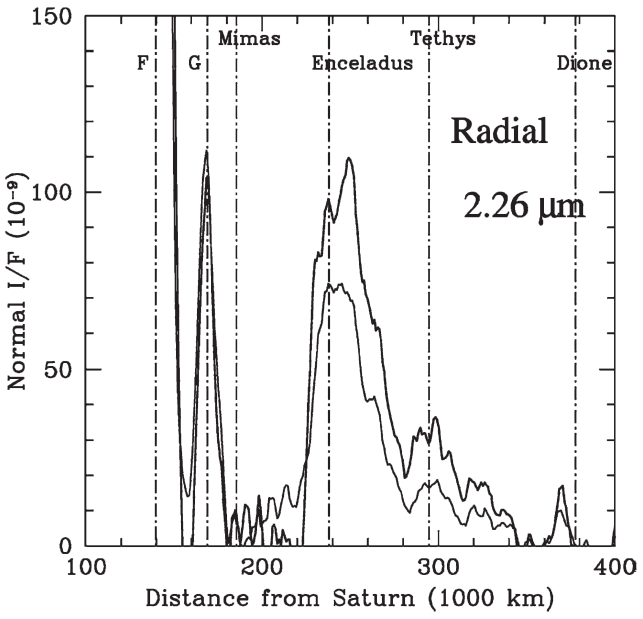

Fig. 16.2 Radial profiles of the back-lit ring derived from Keck near-infrared observations at a wavelength $\lambda = 2.26\,\mu$m. The upper (*heavy line*) profile is vertically integrated over the ring's entire height (0.5 R_S, or 30,000 km), while the lower (*thin line*) profile is integrated over 8,000 km. These thicknesses are much greater than the FWHM of the ring as measured by CDA (cf. Fig. 16.11) (from de Pater et al. 2004)

The D ring, lying inside the main rings, could not be imaged during the ring plane crossing, but was detected in an occultation by the star GSC5249–01240 observed on 21–22 November 1995 with HST (Bosh and Olkin 1996). The outer D ring was noted to have a normal optical depth of around 10^{-3}, while the inner D ring, which included the brightest feature observed by *Voyager* (Showalter 1996), had no detectable optical depth. These data were puzzling at the time, but they began to make more sense in the context of *Cassini* observations. In particular, periodic variations observed in the outer D ring would later be interpreted as the first detection of vertical corrugations in this ring (Hedman et al. 2007a).

HST monitored the activity of the spokes starting shortly before the ring-plane crossing in 1995 until October 1998, when spokes were no longer apparent (McGhee et al. 2005). The implications of these observations are outlined below.

16.3 *Cassini* Observations and Current Theories

Cassini has detected dusty material in numerous locations throughout the Saturn system. The remote-sensing instruments have observed dusty regions extending interior and exterior to the main rings, dusty ringlets within gaps in the main rings, and spokes above the B ring. Further from Saturn, both remote-sensing and in-situ measurements provided information about the G ring and about narrow faint rings and arcs associated with several small moons. Finally, the dust detectors have directly sampled the particles in the extensive E ring and those ejected into interplanetary space. The following sections will consider each of these different features in turn, summarizing both the currently available observational data and the present state of theoretical models.

16.3.1 The D Ring

Lying between Saturn and the classical main rings, the D ring is among the most complex of the faint rings. Both *Cassini* images and earlier *Voyager* observations have revealed a number of distinct structures in this region. The *Voyager* spacecraft detected three features designated as ringlets in this region, along with more subtle, quasi-periodic brightness variations (Showalter 1996). At least two of these ringlets were recovered in *Cassini* images, but these data also indicate significant changes in the structure of the D ring over the last 25 years (Hedman et al. 2007a). For example, the brightest feature in the D ring that was present during the *Voyager* observations was a narrow (<40 km) ringlet located

71,710 km from Saturn's center named D72. Images taken by *Cassini* show no narrow ringlet at this location (Fig. 16.3). Instead there is a much broader feature (with a full-width at half-maximum of roughly 300 km and centered around 71,600 km) with a peak brightness that is significantly less than other structures in the D ring. The connection between this structure and the D72 ringlet is unclear, but regardless of whether the ringlet has vanished or transformed into a broader, more diffuse feature, this would be among the largest secular changes in Saturn's rings observed to date.

Noteworthy features in the D ring include not only brightness variations but also trends in the particle size distribution. Various parts of the D ring have very different photometric and spectral properties that almost certainly reflect variations in the shape of the local particle size distributions (Hedman et al. 2007a). In general, regions closer to Saturn have larger

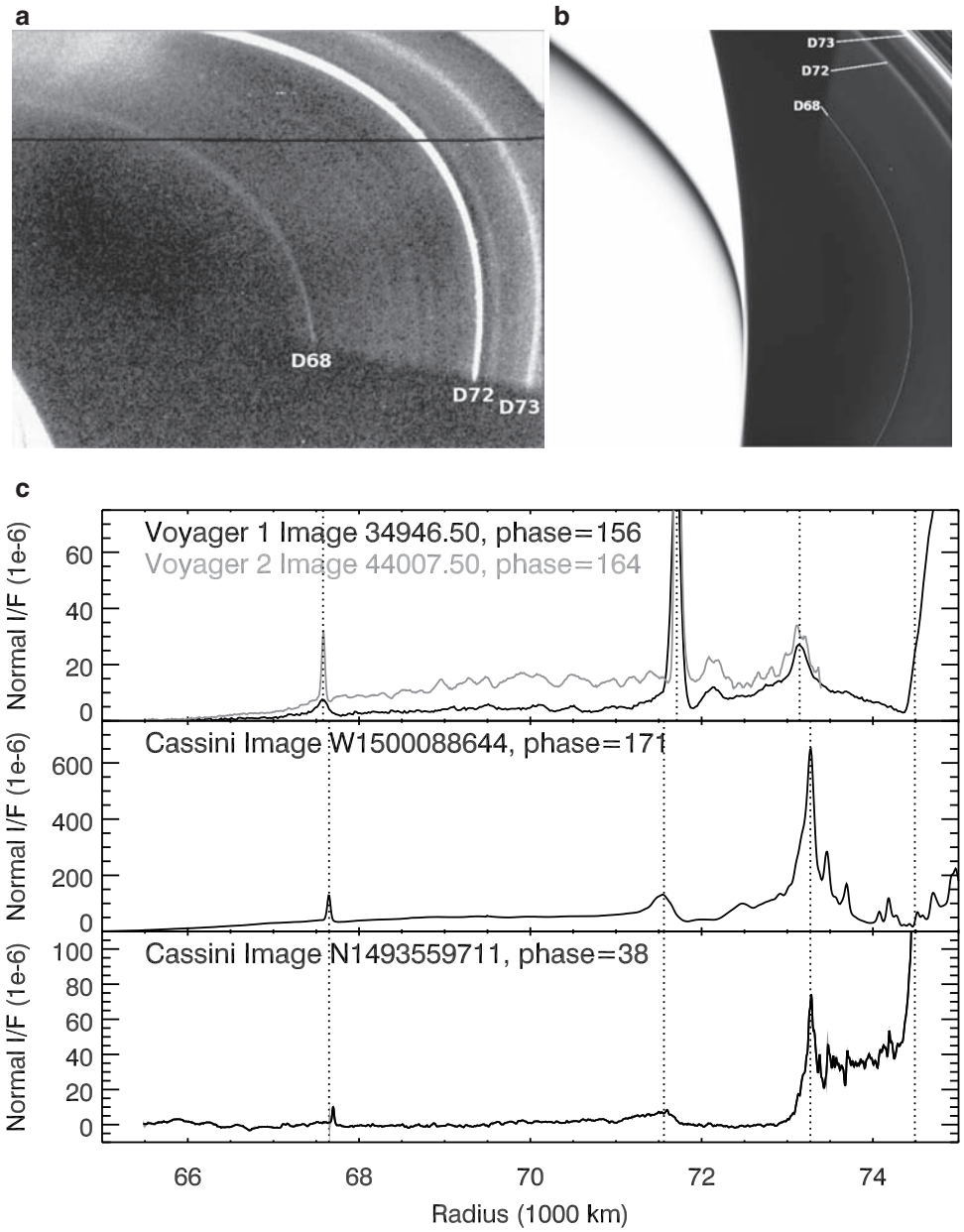

Fig. 16.3 D ring (**a**) *Voyager* image 1 (34946.50) taken at a phase angle of 156°. The three brightest bands were called D68, D72 and D73. The horizontal black line is a data dropout. (**b**) The same region imaged by *Cassini* (W1500088644), at a phase angle of 171°; an over-exposed Saturn fills the image's left half. (**c**) Radial brightness profiles derived from the two images above, a *Voyager* 2 frame (#44007.50 at 164° phase) and an additional *Cassini* image (N1493559711) taken at a phase angle of 38°. The vertical dotted lines mark the positions of D68, D72 and D73 and the C ring's inner edge from left to right (from Hedman et al. 2007a)

fractions of smaller particles (radius of 1–10 μm) relative to larger particles (10–100 μm) compared with regions further out. Moreover, the size distributions vary on more local scales as well. For example, the appearance of the outer part of the D ring (between 73,200 km and 74,500 km) is dramatically different when it was viewed at various phase angles (Fig. 16.3c). At high phase angles, this region appeared to be populated by an array of ringlets, but at low phase angles this entire region seems to be filled with a continuous sheet of material having several brightness minima that look to be correlated with some of the ringlets observed at high phase angles (Hedman et al. 2007a). Likely, non-gravitational processes operate on various scales within this ring to sort particles according to size.

Given this complexity, we consider the various features in the D ring separately, starting from its inner edge and moving outwards. An apparently empty span of about 5,000 km lies between Saturn's cloud-tops and the innermost region of the D ring where material is detectable. This clearing could potentially represent a place where spacecraft could fly close to the planet in order to measure the higher-order components of the planet's gravity and magnetic fields.

Between the inner edge of the D ring at 65,000 km and the inner edge of the D73 ringlet at 73,000 km, there are broad sheets of material that are strongly forward-scattering, implying that they are composed primarily of small particles 1–10 microns across. This may be material derived from the various ringlets that is spiraling inward towards Saturn under the influence of various drag forces.

Embedded in this sheet, roughly 67,650 km from Saturn center is a narrow ringlet called D68. This is the innermost discrete feature in the rings. High-resolution observations of this ringlet reveal that it sometimes has two components, separated by up to 20 km. Lower resolution images indicate the apparent location of this ringlet can vary by up to 50 km, implying that this ringlet is non-circular and/or inclined (Hedman et al. 2007a).

Between 71,000 km and 73,000 km from Saturn center, a region of enhanced brightness occurs around 71,500 km that could be related to the no-longer-visible D72 ringlet seen by *Voyager*, and a local minimum in the surface density appears around 72,000 km. On top of these broad radial structures, there are interesting finer-scale brightness variations that change with time and longitude (see below).

Outside 73,000 km, the character of the D ring changes dramatically: As seen in an occultation (Bosh and Olkin 1996), it has a detectable normal optical depth of 10^{-3} and shows radial brightness variations on scales as small as tens of kilometers. Particularly interesting is a structure that appears as a quasi-sinusoidal variation in the ring's brightness extending between 73,000 and 74,000 km (Fig. 16.4a, Hedman et al. 2007a). Observations of this region at sub-degree ring opening angles show "contrast reversals" similar

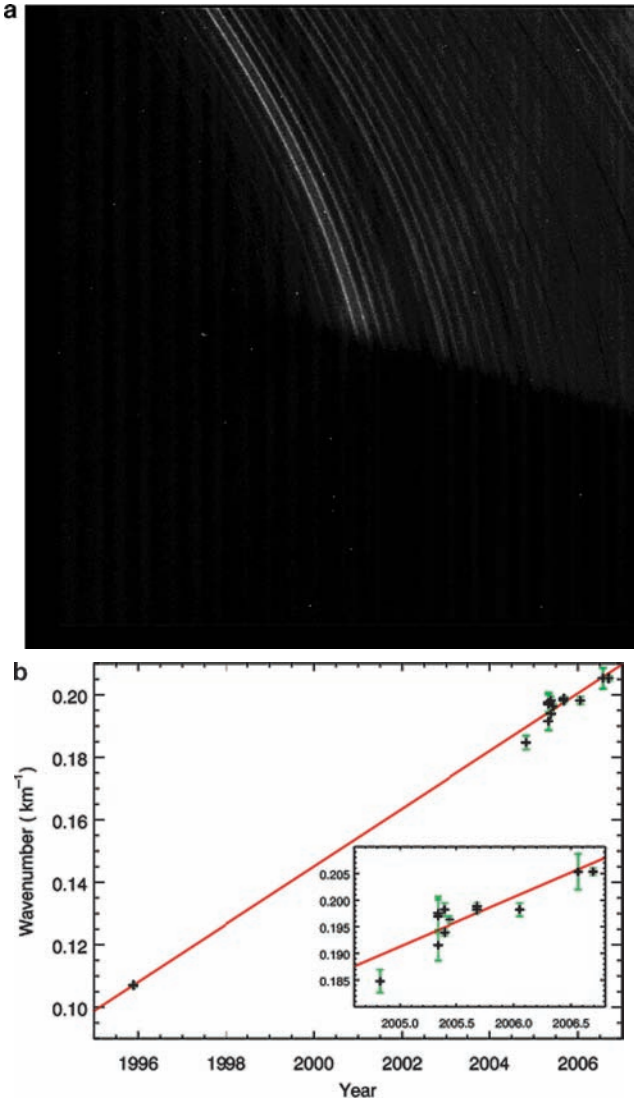

Fig. 16.4 The ∼30-km wavelength structure in the outer D ring. (**a**) One of the highest-resolution images of the outer D ring, obtained at a phase angle of 41° and a resolution of 1.6 km/pixel. The over-exposed inner edge of the C ring lies at the upper right-hand corner of the image, while the shadow cuts across the very lower half of the image. The regular brightness variations in the D ring are apparent, and the ringlet D73 corresponds to the innermost 2–3 brightest features. (**b**) A plot showing the wavenumber $k = 2\pi/\lambda$ of this pattern versus time. The line corresponds to a steady increase in the wavenumber consistent with a progressive winding of the pattern due to differential nodal regression (from Hedman et al. 2007a). This winding up has continued into 2009

to those noted in the Jovian ring (Ockert-Bell et al. 1999, Showalter et al. 2001). These brightness variations can be generated by a vertical corrugation in this part of the D ring. Such a corrugation produces periodic variations in the amount of material along the line of sight that lead to apparent brightness variations in *Cassini* images and optical depth variations in the 1995 occultation data (cf. Gresh et al. 1986).

A comparison of observations taken at different times shows that the wavelength of the corrugation has been

decreasing steadily over time. Specifically, the radial wavenumber $k = 2\pi/\lambda$ has been increasing with time at roughly $2.5 \times 10^{-5}\,km^{-1}\,day^{-1}$ (Fig. 16.4b, Hedman et al. 2007a); this rate has proven to be an excellent predictor of the wavelength into 2009. This steady reduction in the pattern's wavelength can be attributed to differential nodal regression of inclined particle orbits. Extrapolating backwards in time, one can compute when $k = 0$ corresponding to a simple inclined ring, i.e., a plane. The ring would have been in such a state in March 1984. Something, perhaps an impact, may have disturbed this ring at this time.

16.3.2 The Roche Division

Material in the Roche Division was first detected in *Voyager* data (Burns et al. 1984), and *Cassini* observations now show significant substructure in this region (Fig. 16.5). Early *Cassini* observations had seemed to suggest two brightness enhancements near the orbits of the satellites Prometheus and Atlas (Porco et al. 2005). Subsequent observations have indicated that a nearly continuous ring-like structure is present around 139,000 km from Saturn center and just interior to Prometheus's orbit. However, the structure observed near the orbit of Atlas was found to be part of a more complex structure that varies with longitude and time (see below and Hedman et al. 2009b).

16.3.3 Resonant Structures in the D Ring and the Roche Division

Despite one being exterior – and the other interior – to the main rings, the Roche Division and the D ring are connected to each other by a common dynamical phenomenon. In both the inner Roche Division (∼138, 000 km) and in the middle D ring (70,000–73,000 km) complex patterns exist that can be decomposed into multiple series of alternating bright and dark bands tilted relative to the local radial direction (Fig. 16.5). The pattern speeds and morphology of these structures are consistent with patterns generated by multiple Lindblad resonances with periodic perturbing forces (Hedman et al. 2009b). These are reminiscent of the Lorentz resonances, driven by magnetic-field periodicities like those that are important in shaping Jupiter's faint rings (Burns et al. 1985, Hamilton 1994, Ockert-Bell et al. 1999). The forcing periods operating in both regions range between 10.5 and 10.9 h, commensurate with the rotation periods of Saturn's atmosphere (Sanchez-Lavega et al. 2000) and with periods observed in radio emissions (Kurth et al. 2007, Gurnett et al. 2007), but not with the expected periods of acoustic oscillations in Saturn's interior (Marley and Porco 1993). If the forcing in these regions was primarily gravitational, many strong additional resonances would make their presence known in the C ring, and they are not seen. The forcing therefore is more likely due to non-gravitational driving terms, so the dynamics of particles in these regions could

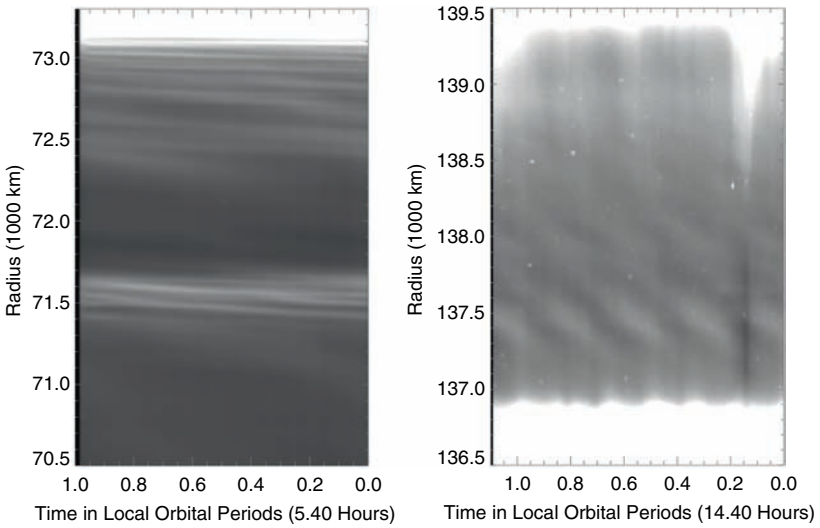

Fig. 16.5 Maps of the D ring (*left*) and Roche Division (*right*) derived from observations taken at high phase angles (∼160°), showing the brightness of these regions at a fixed longitude versus radius and time (note time increases to the left). In the D-ring image, longitudinal brightness variations can be clearly seen around 71,500 km and between 72,500 km and 73,000 km. These patterns are attributed to resonances with asymmetries in Saturn's magnetosphere. In the Roche Division image, the bright streaks near the top of the image are due to bright features in the F ring. A brightness concentration can be seen around 139,000 km (just interior to the orbit of Prometheus), and a periodic structure is visible near 137,500 km (close to the orbit of Atlas). The latter also seems to be produced by asymmetries in Saturn's magnetosphere (from Hedman et al. 2009b)

potentially provide insight into the various asymmetries in the magnetosphere and their influence on small dust grains.

16.3.4 Faint Ringlets Within Main-Ring Gaps

A number of largely empty gaps can be found throughout Saturn's otherwise dense main rings (see Chapter 13). Four of these gaps contain low optical depth ringlets that are strongly forward-scattering (i.e., they are particularly bright in backlit images like Fig. 16.1) and therefore seem to be composed primarily of small ($<100\,\mu$m) particles. Despite containing very little total mass, such ringlets interest modelers because their presence in otherwise open gaps may provide hints as to the mechanism that clears those gaps. In order of increasing distance from Saturn, the ringlet-containing gaps are the Maxwell Gap in the C-ring ($\sim$87,420 km from Saturn center), the Huygens and Laplace Gaps in the Cassini Division ($\sim$117,740 km and $\sim$119,940 km from Saturn center, respectively), and the Encke Gap in the A ring ($\sim$133,590 km from Saturn center). Example Images are displayed in Fig. 16.6.

The Maxwell, Huygens and Laplace gaps each contain a single dusty ringlet in the space between the gap's inner edge and the innermost edge of the optically thick ringlet that occupies each gap (Fig. 16.6 **a–c**; Porco et al. 2005, 2006). These dusty ringlets do not show strong variations in brightness with longitude. By contrast, the dusty material in the Encke Gap has a much more complex structure, being organized into three narrow ringlets (referred to here as the "inner", "central" and "outer" Encke Gap Ringlets) plus another broader, fainter feature known as the "fourth" ringlet (Fig. 16.6 **d**, Porco et al. 2005). The inner, central and outer Encke Gap ringlets all contain "clumps", localized regions that are up to an order of magnitude brighter than the background ringlet; these are associated with "kinks" in the radial position of the ringlet (Ferrari and Brahic 1997, Burns et al. 2005). While the morphology of individual clumps may vary and the clumps in a given ringlet may drift slowly relative to each other, the overall distribution of the clumps in each ringlet has been remarkably persistent over the course of the *Cassini* mission to date. Undulations in the radial position of the inner ringlet have been noted, and these are likely due to the same gravitational perturbations that produce the curious and confounding periodicities on the edges of the Encke Gap.

Many aspects of the origin, evolution and dynamics of these dusty ringlets remain obscure. For example, it is not obvious why the Encke Gap has three or four dusty ringlets while the other gaps have only one. However, comparisons among these features reveal some interesting aspects of these ringlets' behavior. For instance, the spaces occupied by these ringlets are the widest gaps in the rings, and in fact every open space in the main rings wider than 100 km across seems to contain a dusty ringlet. While some narrower gaps contain low optical depth ringlets, open spaces with a mean width less than 100 km do not contain forward-scattering *dusty* ringlets with $\tau \geq 10^{-4}$. This may be related to the fact that most of the dusty ringlets are non-circular. In particular, the ringlet in the Laplace gap exhibits "heliotropic" behavior, where the geometric center of the ringlet is displaced towards the Sun (Hedman et al. 2007c). This ringlet also appears to be inclined and/or displaced out of the ringplane (Burt et al. 2008). This behavior can be explained in part by the perturbations to the particle orbits induced by solar radiation pressure, and similar phenomena are probably operating on some, if not all, of the other dusty ringlets. Non-gravitational

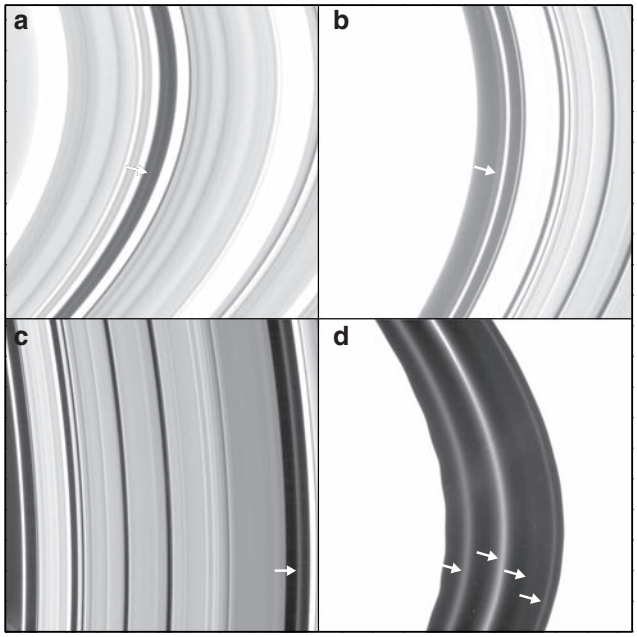

Fig. 16.6 Diffuse ringlets within Saturn's rings. Images (**a**) and (**b**) were taken with a solar incidence angle of 114.5°, an emission angle of 99°, and a phase angle of 145°. (**a**) Image centered on a radius of 84,394 km, has a radial scale of 7 km per pixel, and shows a radial region of 4,290-km extent, including the Maxwell gap in the C ring. The arrow points to a diffuse ring lying interior to the dense Maxwell ringlet. (**b**) This image is centered on a radius of 117,292 km, has a radial scale of 7 km per pixel, and covers 3,870 km, including the Huygens gap immediately outside the outer B-ring edge. The arrow points to a diffuse ring lying interior to the dense Huygens ringlet. Image (**c**) was taken at a phase angle of 111°, an emission angle of 108°, and has a resolution of 2.4 km per pixel centered on 118,907 km, covering a range of 2,571 km, including the Laplace Gap in the outer *Cassini* Division. The arrow points to a dusty ringlet that lies inside this gap. Image (**d**) is from the dayside orbit insertion sequence and is centered on a radius of 133,557 km interior to the Encke gap, has a radial scale of 1.15 km/pixel, a radial extent of 858 km, and was taken from a phase angle of 134°. The arrows point to (from the *left*) the inner, central, fourth, and outer Encke gap ringlets (Images **a**, **b** and **d** from Porco et al. 2005, Image **c** from PIA 08330)

forces like solar radiation pressure are therefore having a significant effect on the shape and structure of these rings. If successfully modeled, these distorted ringlets could provide otherwise unobtainable information on the rings' electrodynamic environment.

16.3.5 Spokes in the B Ring

Spokes are intermittent, approximately radial markings on Saturn's B ring, thought to consist of small charged dust particles lofted from their parent ring bodies owing to electrostatic repulsion. While they were first recognized in images taken by *Voyagers 1* and *2* (Smith et al. 1981, 1982), spokes were possibly noticed earlier in ground-based observations (Robinson 1980) (Fig. 16.7). These perplexing features have attracted great attention; following their appearance in *Voyager 1* images, *Voyager 2*, during its approach to Saturn, dedicated sequences to spoke observations, providing an invaluable dataset. The spokes' characteristics have been derived with an increasing level of sophistication since their acquisition in these images. The desire to provide an explanation for the spokes has played a large role in the emergence of the research field of 'Dusty Plasmas'.

The key physical characteristics of spokes based on the *Voyager* data (Porco 1983, Grün et al. 1983, 1992, Eplee and Smith 1984, Doyle and Grün 1990) can be summarized as follows: These features are generally most common surrounding the dawn ring ansa, and seem to form primarily in that region. Spokes develop on a timescale of minutes, and can become more intense over a period of a few hours. Appearing at radial distances that are near to, or straddle, kronosynchronous orbit, they move around the ring nearly co-rotating with the planet. During increases in spoke intensity, these features extend forwards and backwards from the kronosynchronously moving longitude inside and outside the co-rotation distance, respectively, while their central

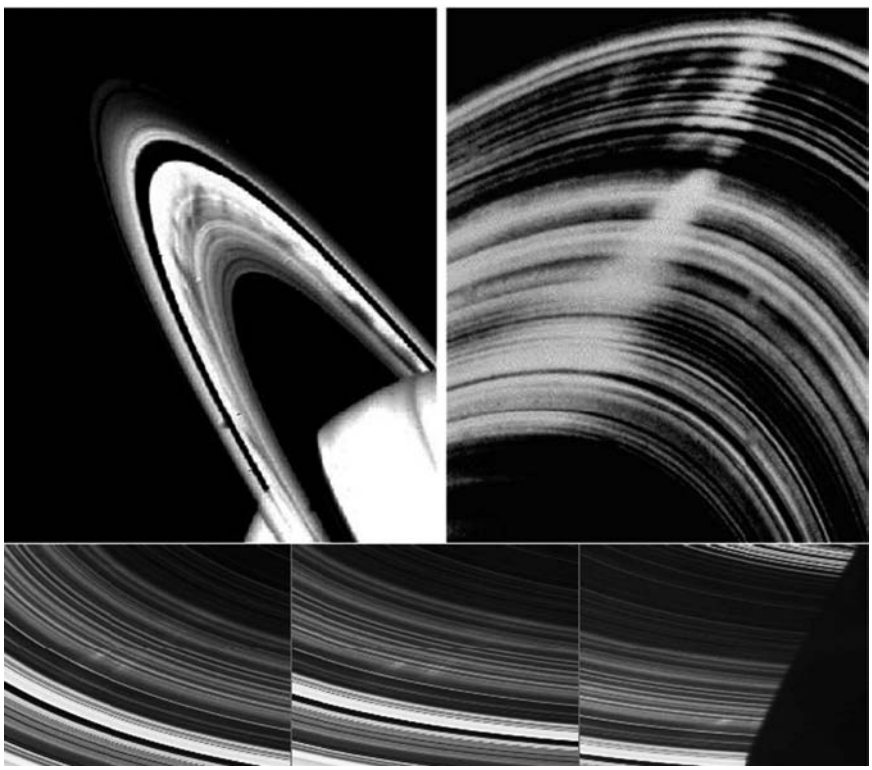

Fig. 16.7 *Top*: Spokes in the B ring as seen by *Voyager* 2 (Smith et al. 1982). The left image was captured in back-scattered light before closest encounter, with the spokes appearing as dark radial features across the ring's center. The right image was taken in forward-scattered light after the spacecraft crossed the ring plane, and was looking back towards the Sun; the spokes now occur as bright markings. Typical dimensions of these spokes are 10,000 km in length and 2,000 km in width. The nature of the changing brightness indicates that spokes consist of small grains with radii ($<1\,\mu$m), i.e., that are comparable to the wavelength of visible light. At the time these images were taken, the rings' opening angle to the sun was $B' = 8°$. *Bottom*: The initial spoke observations by taken *Cassini* on September 5, 2005 ($B' = 20.4°$), over a span of 27 min. These faint and narrow spokes were seen from the un-illuminated side of the B ring. These spokes are $\approx$3, 500 km long and $\approx$100 km wide, much smaller than the average spokes seen by *Voyager*. These images were taken with a resolution of 17 km per pixel at a phase angle of 145° when *Cassini* was 13.5° above the unlit side of the rings as the spokes were about to enter Saturn's shadow (from Mitchell et al. 2006)

regions intensify; this indicates that the spoke material follows Keplerian trajectories, in broad terms at least. Once spokes no longer intensify, they fade while traveling around the day-side of the rings. Newly formed spokes in the *Voyager* data often coincided with the positions of older spokes that seem to have survived an entire revolution around Saturn. This periodicity in spoke formation, with a period near that of the Saturn Kilometric Radiation (SKR) measured by the *Voyagers* (Porco and Danielson 1982), suggests a formation trigger that is linked to Saturn's magnetic field.

As summarized below, numerous formation theories were proposed to explain the spokes' existence, but none could be definitively tested without further observations. HST monitored spoke activity from shortly before the ring-plane crossing in 1995 until October 1998, when HST no longer detected spokes. McGhee et al. (2005) proposed that spokes were possibly always present, but only detectable when the observer lay close to the ring plane. It was therefore anticipated that *Cassini* would detect spokes on its 2004 arrival at Saturn and that its observations would finally decide which, if any, of the competing theories were correct (Horányi et al. 2004). However, contrary to predictions, *Cassini* did not observe spokes, even when close to the ring plane, until September 2005 (Fig. 16.7). The variability in spoke occurrence in HST data was therefore not an observational effect: spokes are indeed a seasonal phenomenon, and their formation can be suspended for extended periods (Fig. 16.8). This seasonal variation of spoke activity may be a consequence of the variable plasma density near the ring. The plasma density is a function of the solar elevation angle B′, measured from the ring plane, since it is generated mainly from the rings by photoelectron production and by photo-sputtering of neutrals that are subsequently ionized (Mitchell et al. 2006, Farrell et al. 2006). Although this may explain the seasonality of spoke activity after their formation, we still lack a generally accepted model for how they are triggered.

Spokes comprise dust particles in a narrow size distribution centered at about $s \sim 0.6\,\mu\mathrm{m}$ (Doyle and Grün 1990). It is generally believed that spoke formation involves charging and thus electric felds acting on these small grains, but this process requires – as we show below – a much higher plasma density than is commonly expected near the rings (Hill and Mendis 1982, Goertz and Morfill 1983). When formed, spokes initially cover an approximately radial strip with an area of $A \sim 10^3 \times 10^4\,\mathrm{km}^2$, with a characteristic optical depth of $\tau \sim 0.01$. The total number of elevated grains can be estimated to be on the order of $N_\mathrm{d} \sim A\tau/\left(\pi s^2\right) \sim 10^{23}$. If the grains are released approximately at the same time and carry just a single electron when released from their parent bodies, the formation of the spoke cloud requires a minimum surface charge density (measured in units of electron charges e) $\sigma_\mathrm{e}{}^* = N_d/A \sim 10^6\,\mathrm{cm}^{-2}$, orders of magnitude higher than the charge density, σ_o, expected from the nominal plasma conditions in the B ring.

The nominal plasma environment near the optically thick B ring is set by the competing electron and ion fluxes to and from the ring due to photoelectron production from the ring (as well as the ionosphere) and the photo-ionization of the rings' neutral atmosphere that is maintained by photo-sputtering. All of these are expected to show a seasonal modulation with the ring's opening angle with respect to the Sun, B′. The characteristic energy for photo-scattered electrons is

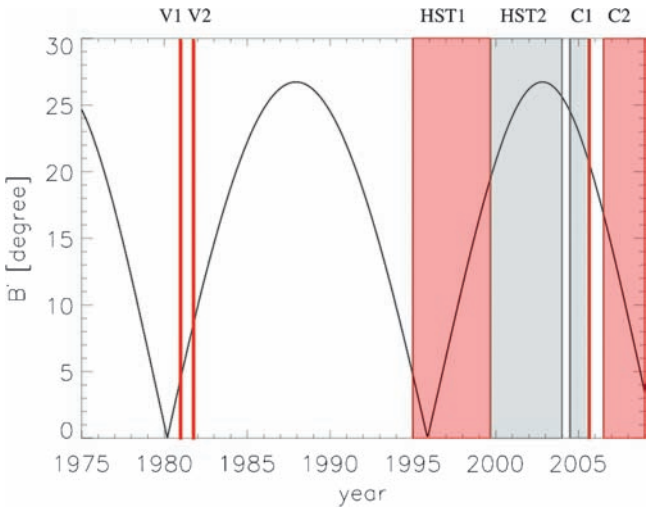

Fig. 16.8 The variation of the absolute value of solar elevation angle B′ as a function of time. Red lines and red-shaded areas identify when spokes were visible. The vertical red lines V1 and V2 indicate the *Voyager* encounters in 1980 and 1981. HST1 and HST2 mark the periods of spoke observations by HST (McGhee et al. 2005). C1 shows the period without spoke activity as reported by *Cassini* following its orbit insertion in June 2004, ending with its first spoke sighting in September 2005. C2 is the current episode when spokes are active. Due to *Cassini*'s low inclination orbit between September 2005 and July 2006, spokes could not be observed

$T_e \sim 2\,\mathrm{eV}$, and the plasma density is expected to be $n \sim 0.1-1\,\mathrm{cm}^{-3}$ (Waite et al. 2005). The characteristic plasma shielding distance is $\lambda_D = 740\ (T_e/n)^{1/2} = 1-3\times10^3\,\mathrm{cm}$, larger than the average distance between the cm - m sized objects in the B ring, which has a comparable vertical thickness, $h \sim 10\,\mathrm{m}$. Hence, it is reasonable to treat the B ring as a simple sheet of material (Goertz and Morfill 1983). The nominal surface potential, including its possible seasonal variations, is expected to be in the range of $-5\,\mathrm{V} < \phi_R < 5\,\mathrm{V}$. The surface charge density can be estimated from Gauss's law,

$$\sigma_o \sim \varphi_R/(4\pi e\lambda_D) \sim 2.5\,\phi_R\,(n/T_e)^{1/2} < 1-3\times10^3\,\mathrm{cm}^{-2}.$$

Since $\sigma_o << \sigma_e{}^*$, the formation of a spoke requires higher than normal plasma densities.

Several spoke formation theories, as described by McGhee et al. (2005), have been put forward. Of these, the proposed spoke formation trigger theories that arguably have been most widely accepted are those of meteoroid impacts onto the rings (Goertz and Morfill 1983) and field-aligned electron beams originating from the auroral regions of Saturn (Hill and Mendis 1982): both could transiently increase the plasma density above a critical threshold, and trigger the formation of spokes.

A meteoroid impact-produced plasma cloud was shown to expand, cool and recombine as it rapidly propagates in the radial direction, possibly explaining many of the observed spoke characteristics. However, the estimated propagation speed of such a cloud seems to have been overestimated (Farmer and Goldreich 2005, Morfill and Thomas 2005). An electron-beam mechanism has been suggested to loft small particles instantaneously along the entire radial extent of a spoke (Hill and Mendis 1982). Other spoke formation ideas include dusty plasma waves (Tagger et al. 1991, Yaroshenko et al. 2008) and impact-induced avalanches of small charged dust particles (Hamilton 2006). *Cassini* image sequences with high-temporal resolutions could easily determine the radial propagation speed of a forming spoke, but such sequences have not yet been obtained (Mitchell et al. 2008).

Recently, an alternative formation process has been proposed which suggests that, although the electrostatic charging mechanism is responsible for spoke formation as first postulated by Hill and Mendis (1981), the exact cause of the charging is linked to electrical storms in the atmosphere of Saturn itself (Jones et al. 2006). Following a terrestrial lightning discharge, strong electric fields are thought to exist above the associated thunderstorms. The ionization of atmospheric particles by incoming cosmic rays, in the presence of this electric field, can set off an electron avalanche, as has been suggested to cause gamma-ray emission from above thunderstorms. When the atmospheric density is low enough, such electron avalanches can escape into the magnetosphere (e.g., Lehtinen et al. 2000). The escaping electrons are guided by the planetary magnetic field to the thunderstorm's magnetic conjugate point in the opposite hemisphere. At Saturn, if this occurs within a certain range of latitudes, the escaping electrons will strike the rings and possibly trigger spokes. The ionospheric density varies with local time, and reaches a minimum near local dawn (Moore et al. 2004), where spoke formation is indeed most prevalent.

Although radio emissions, termed Saturn Electrostatic Discharges (SEDs), are known to be linked to Saturnian thunderstorms (Burns et al. 1983, Fischer et al. 2006), the detection of whistler radio waves in the absence of an SED (Akalin et al. 2206) suggests that SEDs may not be as reliable markers of thunderstorms as previously concluded from *Voyager* observations. *Cassini*'s MIMI instrument (Krimigis et al. 2004) has detected a pair of magnetic field-aligned electron beams (Jones et al. 2006), which in many respects are similar to those expected from thunderstorms (Lehtinen et al. 2000). No accompanying observation of SED emission or whistler events were noted during this time, so a link with thunderstorms remains unproven.

During the first four years (2004–2008) of *Cassini* observations, spokes remained a high priority. For most of this interval, spokes were much fainter and less frequent than those seen by the *Voyagers* (Fig. 16.8). By late 2008, B′ had reached values similar to those during the *Voyager* encounters, and spoke activity was indeed approaching - if not matching - the activity observed by the *Voyagers* (Mitchell et al. 2008). Some observations suggest that a periodicity linked to the SKR emission period is appearing again. Based on the increase in spokes at the time of writing, it is anticipated that *Cassini* should answer key questions regarding the nature of these perplexing ring features around the equinox period of 2009–2010.

16.3.6 The G Ring

Several relatively narrow rings reside between the F ring and the core of the E ring. The brightest and best known of these is the G ring, located approximately between 165,000 and 175,000 km from Saturn center; the exact boundaries of this ring are difficult to define precisely as its edges blend smoothly into the background E ring. This ring has an asymmetrical profile, with a sharp inner edge and a diffuse outer boundary. Near the inner edge of this ring, at 167,500 km, a bright arc of material extends over roughly 60° in longitude, with a peak brightness several times that of the background G ring and a radial full-width at half-maximum of approximately 250 km (Fig. 16.9). This arc has been observed multiple times over the course of the *Cassini* mission, indicating that it is a persistent feature in the G ring. Furthermore, these observations allow us to measure the mean motion of this

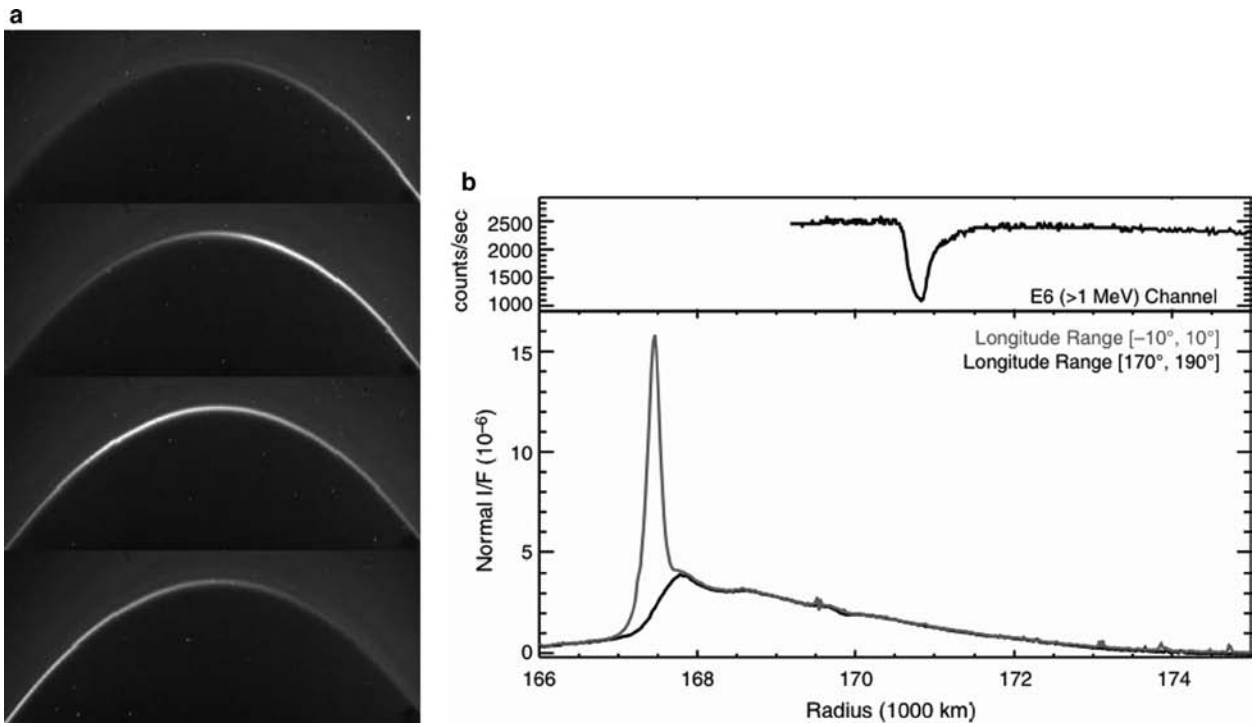

Fig. 16.9 (**a**) Images of the G ring arc obtained on September 19, 2006 at 12:37, 13:11, 13:44, and 14:18 UTC from top to bottom. The bright arc moves from right to left through the field of view. (**b**) *Top*: The drop-out in charged-particle flux detected during *Cassini*'s passage over the arc region on September 5, 2005. The radial scale corresponds to the equatorial distance of the unperturbed magnetic field lines that thread *Cassini* at the time of the observation. *Bottom*: Average (offset-subtracted) radial brightness profiles of the G ring at different longitudes relative to the arc's peak visible in **a**. The profiles through the arc (grey) and elsewhere (black) are essentially identical outside 168,000 km, whereas the arc has a sharp peak at 167,500 km. The absorption feature's radial width is comparable to that of the visible arc. While the absorption is radially displaced from the arc, this may be explained by larger-scale magnetospheric processes or through deformations in the magnetic field by the arc (from Hedman et al. 2007b).

feature. This arc lies near the 7:6 co-rotation eccentricity resonance with the moon Mimas, suggesting that this resonance is likely responsible for confining the arc in longitude. Indeed, numerical models of the motions of particles trapped in this resonance can reproduce the arc's observed radial and longitudinal extent (Hedman et al. 2007b).

On 5 September 2005, *Cassini* flew through the magnetic field lines that pierced the arc. During this passage, the MIMI experiment detected a strong, ∼50% depletion in energetic electrons (Fig. 16.9b). Although a subtle energetic proton macrosignature is always present in association with the G ring, and indeed was observed by Pioneer 11 before the ring was identified in images (Van Allen et al. 1983, and references therein), such a deep depletion was not present in previous passages near the G ring, implying that the absorption was due to material trapped in the arc. Like some other microsignatures of small satellites in this region of Saturn's magnetosphere (cf. Roussos et al. 2008), the G-ring's absorption is displaced radially (see Fig. 16.9b), possibly because of local currents (cf. Thomsen and Van Allen 1980; Roussos et al. 2007). The magnitude of the absorption indicates that the arc contains a total mass between 10^8 and 10^{10} kg, equivalent to a 100-meter-wide ice-rich moonlet (Hedman et al. 2007b). In fact, a small sub-kilometer moonlet Aegaeon was recently observed embedded in the G ring arc (Porco et al. 2009). Given the breadth of the absorption feature observed by MIMI, and the fact that the cross-section of this object is much less than the total cross section of large particles computed by Van Allen (1987), it is unlikely that Aegaeon is the only absorbing object in this region. Instead, Aegaeon probably shares the arc with a population of particles between 1 and 100 m across.

While the larger particles are likely resonantly confined to the arc by Mimas's action, the dust they produce has stronger interactions with the ambient plasma and therefore can escape to produce the rest of the visible G ring. Since the local orbital speed is lower than the speed of the plasma (which co-rotates with the magnetosphere), interactions between the dust and plasma will tend to accelerate the dust grains and cause them to drift away from Saturn (Burns et al. 2001). As the particles move outwards, they are eroded by processes like sputtering, causing the density of material to decline with distance from the arc. Such a model would explain why the bulk of the G ring lies exterior to the arc, and can

even account for the presence of relatively large particles throughout the G ring, consistent with the detection of a large (>100 micron) grain around 176,700 km by the dust detector (Hedman et al. 2007b).

16.3.7 Other Narrow Outer Faint Rings

Just as the bodies in the arc can provide a source for ring material in the G ring, small moons can also potentially supply material to narrow rings (Burns et al. 1999, 2001). Thus far, diffuse rings have not been noticed in the vicinity of Daphnis in the Keeler Gap or around the Lagrangian moons of Tethys and Dione. However, diaphanous rings have been observed near several small moons that reside between the F ring and Enceladus. In extremely high-phase imaging of the region around the G ring, at least two rings were discovered. A relatively broad feature is found surrounding the orbit of the co-orbital moons Janus and Epimetheus, and another ringlet overlaps the orbit of the small moon Pallene (Porco 2006, Hedman et al. 2009a).

The highest-phase images did not show clear evidence for ringlets associated with two other small moons of Saturn, Methone and Anthe. However, in-situ measurements and subsequent images demonstrate that these moons are also embedded in tenuous arcs of material. Roussos et al. (2008) reported >0.6 MeV electron microsignatures detected by *Cassini*'s MIMI instrument on 2006 September 9, approximately centered at equatorial distances of 3.23 and 3.31 R_s. The former was detected when *Cassini* was ~12,000 km from Methone, at the exact orbital distance of the moon. Although Methone is only ~3 km wide (Spitale et al. 2006), the microsignature width measured ~1,500 km. Radial diffusion could account for a signature up to ~100 km wide; the observed signature therefore suggests the presence of an arc of material sharing an orbit with Methone. Given the 3.31 R_s microsignature's relatively close proximity to Methone, it too may be associated with that moon, but that signature would have been displaced radially due to magnetospheric currents (e.g. Hedman et al. 2007b). We note that the more distant signature's equatorial radius is close to the orbit of Anthe, a moon measuring approximately 1 km in diameter (Cooper et al. 2008). However, as the latter moon was separated from *Cassini* by ~131°, it is more likely that Methone and its putative arc of material was again the cause. Imaging data later confirmed the existence of an arc of material extending ±5° in longitude around Methone (Fig. 16.10, Hedman et al. 2009a).

These images also demonstrate that an arc of material extending over 20° in longitude surrounds Anthe (Fig. 16.10, Hedman et al. 2009a). Both these moons are trapped in co-rotation eccentricity resonances with Mimas (Spitale et al. 2006, Cooper et al. 2008, Hedman et al. 2009a), and the longitudinal extents of these arcs are consistent with them being resonantly trapped populations of particles. These arcs are therefore directly analogous to the G-ring's arc. Comparisons among these different rings and their relationships with their parent bodies therefore promise to be very productive, especially since the range of parent-body sizes involved brackets the ~10 km "optimal size" for dust production derived by Burns et al. (1984, 1999).

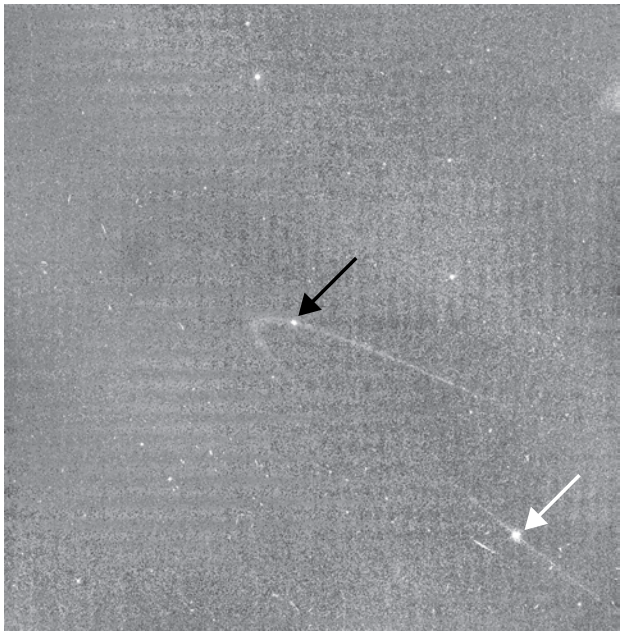

Fig. 16.10 Image showing arcs of debris associated with the small moons Anthe (*black arrow*) and Methone (*white arrow*) (from Hedman et al. 2009b)

16.3.8 The E Ring

The E ring is the most extensive planetary ring in the solar system, enveloping the icy satellites Mimas, Enceladus, Tethys, Dione, Rhea and, as *Cassini* has discovered, Titan. Since the maximum edge-on brightness occurs near Enceladus's mean orbital distance, the icy moon was early on proposed to be the dominant source of ring particles (Baum et al. 1981). In telescopic data, brightness enhancements were suggested to occur also near Tethys (de Pater et al. 1996, 2004) and Dione (Baum et al. 1981), but are not apparent in *Cassini* data. Ever since the ring's discovery (Feibelman 1967), it has been mainly investigated using ground- and space-based images. Through such analysis, a global description of the ring was achieved (Showalter et al. 1991). More recently, the ring has been extensively imaged by the remote-sensing instruments onboard the *Cassini* spacecraft (e.g., Fig. 16.1).

In-situ spacecraft measurements in the Saturnian system provide a complementary view of the E ring by measuring dust impacts during passages through the ring. *Voyager 1*'s planetary radio-astronomy (PRA) and plasma-wave (RPWS) instruments were first to identify dust impacts by their characteristic electromagnetic signatures, as the spacecraft traversed the E ring in 1980 (Aubier et al. 1983, Gurnett et al. 1983, Meyer-Vernet et al. 1996). The Cosmic Dust Analyzer (CDA) onboard *Cassini* is the first dedicated dust detector to investigate the local properties in the E ring, including the spatial and size distributions of the dust particles, their charge state, as well as their chemical composition (Srama et al. 2004). By the end of 2006, *Cassini* performed two almost equatorial and eleven steep traversals through the E ring inside the orbit of Dione in a favorable configuration for dust measurements. Steep passages through the ring plane are particularly useful for determining the ring's vertical profile where the ring-plane is pierced (Fig. 16.11). Unfortunately, little similar vertical data has been obtained since 2006; in fact, because of the primary instrument (HRD) was partially damaged on *Cassini*'s closest passage to the G ring, it is unlikely that data of this quality will be obtained in the near future.

These new data must be interpreted in the context of the discoveries that Enceladus is a geologically active moon, and that the plume of particles launched from the vents at Enceladus' south pole is likely the primary source for most of the E ring. Enceladus and its plume are described in detail in other chapters in this book, but for completeness, we briefly review the findings relevant to the E ring here. From the plume's brightness profile, Porco et al. (2006) concluded that about 1% of the particles, ejected with a mean velocity of $60\,\mathrm{m\,s^{-1}}$ escape at a rate of about 10^{13} particles $\mathrm{s^{-1}}$ $\left(0.04\,\mathrm{kg\,s^{-1}}\right)$ to the E ring, while Spahn et al. (2006) inferred from the dust data that about $5 \cdot 10^{12}$ particles larger than $2\,\mu\mathrm{m}$ escape from the moon's gravity – amounting to an escaping dust mass of at least $0.2\,\mathrm{kg\,s^{-1}}$. The latter authors also constrained the escape rate of ejecta particles created by

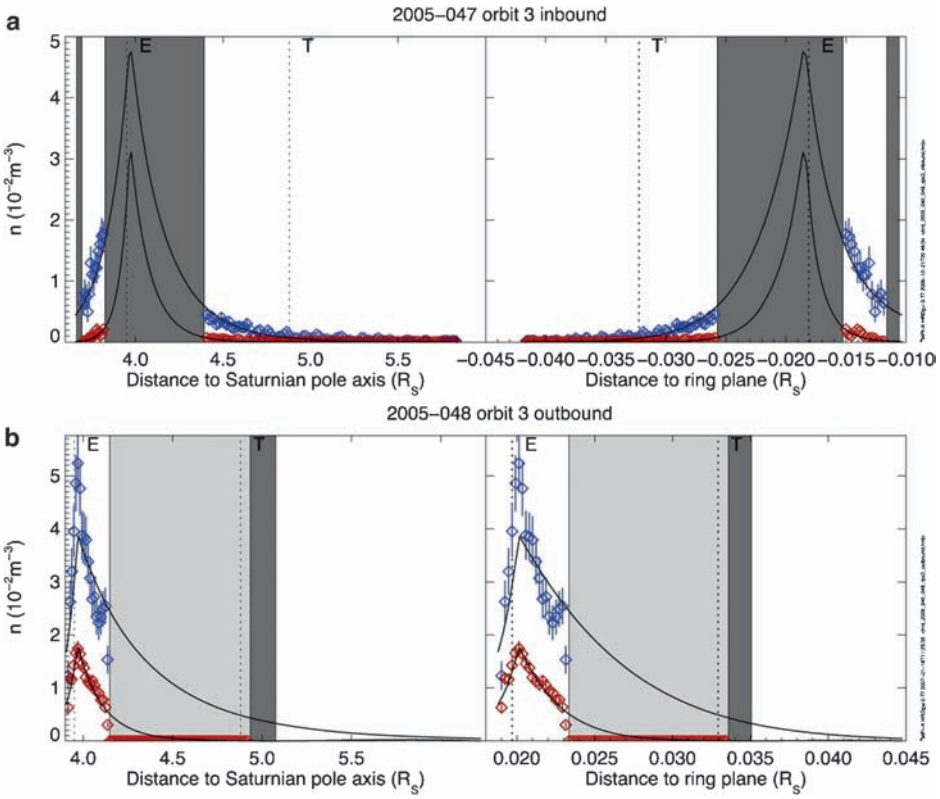

Fig. 16.11 Spatial distribution of E-ring particles with radii $s \geq 1.3\,\mu\mathrm{m}$ (blue) and $s \geq 2.4\,\mu\mathrm{m}$ (red) inferred from CDA measurements inside 6 R_S (364,000 km) during *Cassini* orbit 3. The dust number density versus distance to Saturn's rotation axis (*left*) and versus the elevation above the ring plane (*right*) for the (**a**) inbound, and (**b**) outbound segments of the trajectory. Light grey areas mark periods when the detector was either insensitive to E-ring dust particles or the data were not transmitted to Earth; areas in dark grey indicate periods when the instrument's operation interfered with data acquisition. The curves show the empirical model presented in the text. The dotted vertical lines labeled E and T show the positions of the satellites Enceladus and Tethys (from Kempf et al. 2008).

hypervelocity impacts of interplanetary meteoroids (Krivov et al. 2003) or E ring particles (Hamilton and Burns 1994) onto the moon's surface to be at most 10^{12} particles s^{-1}.

Schmidt et al. (2008) suggested that the plume particles nucleate and condense from the water vapor expanding inside fractures in the moon's surface, while the size and speed distributions of the emerging grains are established by wall collisions within the vents before the grains escape to vacuum. By adjusting their model to match the available imaging and in-situ data, they obtained a total dust production rate in the plume of about $5\,kg\,s^{-1}$. The resulting size-dependent speed distributions of the bigger plume particles are consistent with the distributions inferred from infrared spectra of the plume at altitudes ranging between 50 and 300 km (Fig. 16.12), obtained by *Cassini* VIMS (Hedman et al. 2009c). The spectral data provide clear evidence that the gradient of the particles' speed distribution increases with the grain size, implying that bigger grains are predominantly found at lower altitudes. Hedman et al. (2009c) estimate for grains of one-micron radius ejected at $120\,m\,s^{-1}$ a total flux of a few times 10^{18} per m^2 (total number of such grains per second and per velocity increment per size increment). Schmidt et al. (2008) compute about the same flux. Spitale and Porco (2007) showed that the plume is composed of at least eight dust jets emerging from discrete sources localized at thermal hot spots identified by *Cassini* CIRS (Spencer et al. 2006).

The overall structure of the E ring can be described by an empirical model derived from CDA dust measurements interior to Rhea's orbit for grains with s > 0.9 micrometers. This model gives the number density n as a function of the distance r to Saturn's spin axis and the altitude z above the ring's symmetry plane. The radial distribution of ring particles with $s > 0.9\,\mu m$ is reasonably well described by a pair of power laws centered at the densest point within the ring plane, while the vertical ring thickness increases linearly with distance from the densest point:

$$n(\rho, z) = n_0 e^{-(z-z_0)^2/2\sigma^2} \begin{cases} (\rho/\rho_c)^{+e_i}, \rho \le \rho_c \\ (\rho/\rho_c)^{-e_o}, \rho > \rho_c \end{cases}$$

with

$$\sigma(\rho) = \sigma_c + (\rho - \rho_c) \begin{cases} \frac{\sigma_i - \sigma_c}{\rho_i - \rho_c}, \rho \le \rho_c \\ \frac{\sigma_o - \sigma_c}{\rho_o - \rho_c}, \rho > \rho_c \end{cases} \quad \text{and}$$

$$z_0(\rho) = \begin{cases} z_0(\rho_i)\frac{\rho - \rho_c}{\rho_i - \rho_c}, \rho \le \rho_c \\ 0, \rho > \rho_c \end{cases},$$

where $e_i \sim 50$, $e_o \sim 20$, $\sigma_i = 2,293\,km$, $\rho_i = 3.16\,R_S$ (Mimas's orbital semi-major axis), $\sigma_c = 1,826\,km$, $\rho_c = 3.98\,R_S$, $\rho_o = 4.75\,R_S$ (Tethys's semi-major axis), $\sigma_0 = 2,336\,km$, and $z_0(\rho_i) = -1,220\,km$ (see Fig. 16.11). Note that the variables σ and z_0 give the vertical extent and the vertical offset of the ring as a function of ρ.

Densities change by about a factor of two from orbit to orbit; presumably, such changes reflect the time-variability in the plume source, the plasma properties and the magnetosphere's configuration. Also, images like Fig. 16.1 indicate that the color and brightness of the ring is modulated with longitude and/or hour angle, perhaps because particles of various sizes are responding in different ways to the dynamics, as predicted by Hamilton (1993). Thus a radially symmetric model oversimplifies the ring's actual complexity.

The peak number density, according to CDA, was found to be 0.16 to 0.21 m^{-3} for grains with $s > 0.9\,\mu m$ and 0.021 to 0.076 m^{-3} for $s > 1.6\,\mu m$. The in-situ results roughly match the local number densities for $s > 0.9\,\mu m$ derived from the shadows of embedded moons in the E ring seen in *Cassini* images, which were estimated to be about $0.03\,m^{-3}$ in the vicinity of Enceladus, and about a tenth this value at Tethys (Schmidt and Sremčević 2009). The analysis of the shadows is consistent with a local depletion in space number density of grains with radii smaller than about half a micron near the mid-plane of the E ring. This could be a consequence of the rapid orbital evolution of the population of smaller grains and their dispersal over a larger radial and vertical domain.

Remarkably, the location of the densest point does not coincide with Enceladus's orbit but is displaced outwards by at least 3,000 km (Kempf et al. 2008), which is likely due to plasma drag (Juhász et al. 2007). This displacement was noticed earlier in ground-based (Fig. 16.2, de Pater et al. 2004) and HST observations. As seen through these telescopes, the ring's brightness blends with the background at about $7.5\,R_S$ (450,000 km), whereas, according to the impacts on *Cassini*'s CDA, the ring extends to much greater radial distances, engulfing even Titan's orbit. Remarkably, outside Enceladus's orbit, the ring's radial profile decays smoothly until Titan's orbit (Srama et al. 2006). The large spatial extent of the E ring in both the radial and vertical directions was already noted by the RPWS instrument onboard Voyager *1* when it crossed the ring plane in 1980 (Gurnett et al. 1983).

The vertical profiles at Enceladus's orbit derived from the *Cassini* CDA measurements are in good agreement with those derived from RPWS and edge-on images of this ring (Kurth et al. 2006, Kempf et al. 2008). Interior to Enceladus's orbit, the vertical distribution of ring particles with radii $s > 0.9\,\mu m$ is well described by a Gaussian profile in CDA data, but exterior to Enceladus the vertical ring structure no longer shows a Gaussian distribution. Images of the E ring and the RPWS data also indicate that near the orbit of Enceladus the ring has a two-banded vertical structure with maxima occurring ± 1,000 km from the mid-plane (Kurth et al. 2006). The ring's full-width-half-maximum (FWHM) has its minimum of ≈4,200 km at Enceladus and rises to ≈5,400 km by

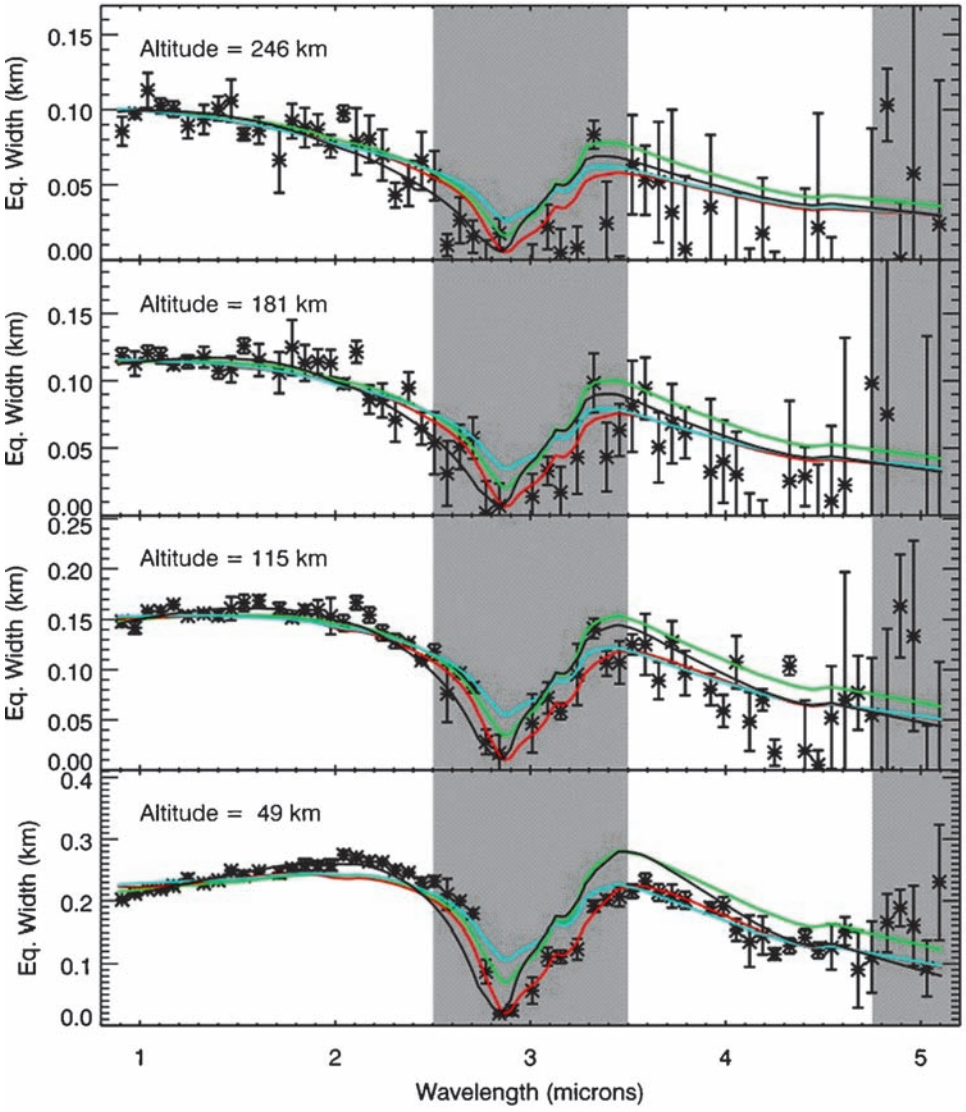

Fig. 16.12 Sample IR spectra of Enceladus's plume derived from *Cassini* VIMS data. The absorption band at 3 microns is due to water ice. Outside this band, the overall slopes of the spectra vary in ways that are sensitive to the size distribution of the ejected ice grains. The black lines are the best-model fits, while the colored lines are scaled spectra for the best-fit size distributions computed using Mie theory for spheres (red) and for irregular shape models 3 (green) and 5 (blue) from Pollack and Cuzzi (1980) (from Hedman et al. 2009c)

Mimas's orbit (Kempf et al. 2008). The ring also flares exterior to Enceladus, and its FWHM at Tethys' orbit is about 5,500 km for grains with $s \geq 1\,\mu m$, and 6,300 km at 4.97 R_S (301,000 km) for grains with $s \geq 0.6\,\mu m$. The ring thickness at Enceladus does not depend on the grain size at least for particles with $s \geq 1\,\mu m$ (Kempf et al. 2008). At Mimas, the ring is displaced southwards by ≈1,200 km with respect to the planet's equatorial plane, while the CDA data provide no evidence for the ring's vertical displacement between the orbits of Enceladus and Dione (some evidence for such displacements may be seen in images like PIA07803, however). The relevance of the directional plume-particle injection for the vertical E ring structure was swiftly recognized (Porco et al. 2006, Juhász et al. 2007). Numerical simulations of particle paths within the jets (Kempf et al. 2009) indicate that the small-scale features apparent in the vertical E ring profiles measured by *Cassini* CDA are associated with specific Enceladus dust jets (Fig. 16.13).

The particle sizes in the E ring found by the CDA experiment are similar to those in the Enceladus plume inferred by the VIMS team. So far, particle size distributions in the E ring have only been obtained for grains with $s > 0.9\,\mu m$. Near Enceladus's orbit, the differential size distribution $n(s)ds \sim s^{-q}ds$ has slopes between $4.2 < q < 5.4$. The slope derived from CDA measurements is generally smaller than the slope derived from the RPWS data (Kurth

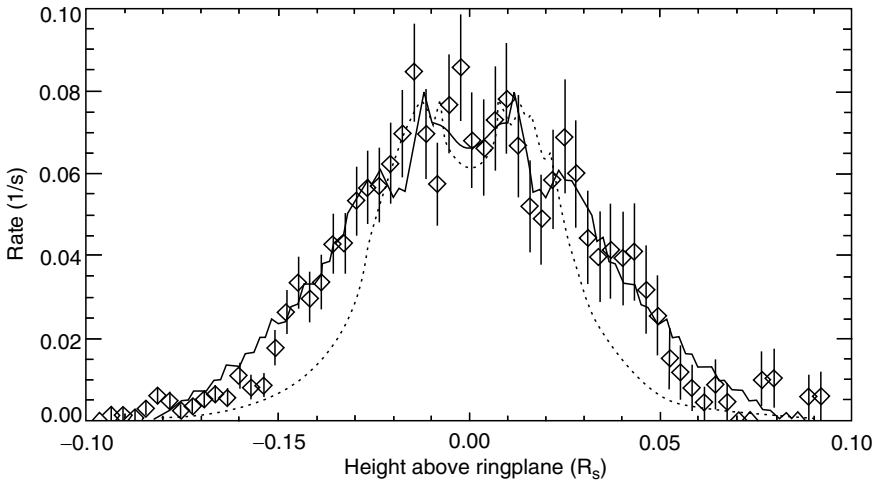

Fig. 16.13 Comparison between the dust impact rate recorded by the *Cassini* dust detector during a steep crossing of the ring plane at a radial distance from Saturn's center of 3.93 R_S (diamonds) and the vertical ring profile resulting from simulations of the Enceladus jet particle propagation (*solid line*). The dotted curve shows the solution of a simple four-parameter model for the inclination distribution for each of the individual jets (from Kempf et al. 2009)

et al. 2006), perhaps because RPWS was not designed to measure dust and, thus, its derived grain sizes may be uncertain. Different parts of the E ring could have different size distributions due to variations in the relative concentrations of freshly ejected plume particles like those measured during the close Enceladus flyby in orbit 11, versus background E-ring particles (Spahn et al. 2006, Kempf et al. 2008).

For the first time, CDA's time-of-flight mass spectrometer allowed the composition of the ring particles to be determined in situ. Measurements obtained during *Cassini*'s initial E-ring crossing in October 2004 have concluded that the particle composition in the outer E ring is dominated by water ice (Hillier et al. 2007). Based on a detailed analysis of 2,000 mass spectra, two major types of ring particles have been identified (Fig. 16.14). Type I spectra show hardly any traces of ions other than the bulk water ice material and a tiny amount of sodium; Type II spectra exhibit impurities of organic compounds and/or silicate minerals within the ice particles (Postberg et al. 2008).

It seems unlikely that water-ice particles with embedded impurities are surface ejecta produced by hypervelocity impacts of interplanetary meteoroids or E ring particles onto Enceladus's clean ice crust (Cuzzi and Durisen 1990). This suggests that Type II dust exclusively originates from Enceladus's ice geysers while Type I particles are surface ejecta (Postberg et al. 2008). The similar composition of Saturnian stream particles (discussed in the following section) and the impurities within the Type II particles suggests that the stream particles are the sputtered remnants of larger E ring particles created in the interior of Enceladus (Kempf et al. 2005b, Postberg et al. 2008). Both particle types can be found in abundance everywhere in the E ring, indicating

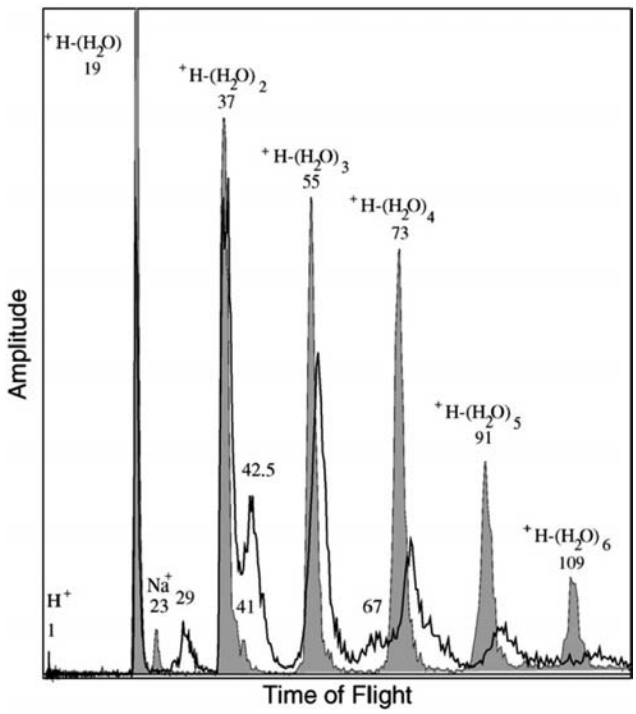

Fig. 16.14 Type I (grey) and Type II (solid line) particle mass spectra. The only non-water features observed in the Type I spectra come from known contaminants (from Postberg et al. 2008)

the rapid dispersal of Enceladus plume particles throughout the entire ring. Two additional minor dust populations consist of sodium-rich water ice (Type III) (Postberg et al. 2009) and of pure minerals (Type IV).

Model calculations for grain growth inside Enceladus's vents show that the trace sodium concentrations in Type I

and Type II particles are in good agreement with the condensation of vapor emerging from liquid water with much higher salt concentrations. However, the high Na content of Type III grains is not consistent with the rapid sublimation of solid ice nor the decomposition of clathrates (Postberg et al. 2009). Consequently, evaporation of a liquid water reservoir below Enceladus's ice crust, which is – or was – in contact with the moon's rocky core, appears to be the most significant plume-producing process.

CDA has also measured the charge of particles in the E ring. Figure 16.15 shows the charges measured on 367 large E-ring particles by CDA early in *Cassini*'s tour (Kempf et al. 2006). We compare these measurements to those calculated for the expected surface potentials on dust using a model of the magnetospheric plasma environment based on *Voyager* measurements (Juhász et al. 2002). Inside 6.5 R_S (394,000 km), all grains carried negative charges, while outside 7.5 R_S (455,000 km) the detected

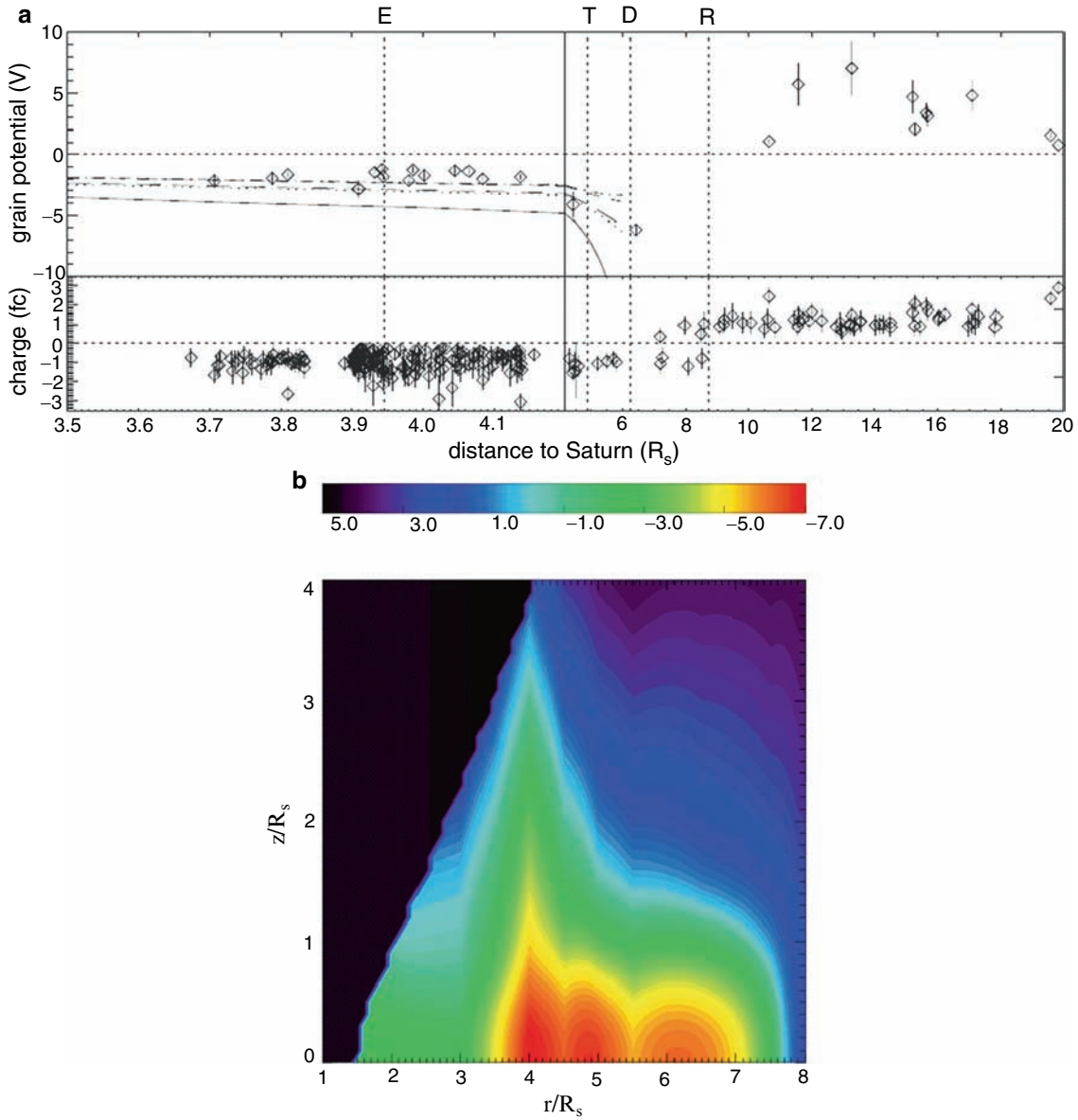

Fig. 16.15 (**a**) The electrostatic grain potential (*upper panel*) and grain charge (*lower panel*) measured by *Cassini*'s CDA as a function of the radial distance to Saturn. The section between 3.5 and 4.2 R_S is displayed on an expanded scale. Dotted vertical lines give the orbital distances of Saturn's moons Enceladus (E), Tethys (T), Dione (D), and Rhea (R). The electrostatic potential is only plotted for impacts having a charge feature with a signal-to-noise better than 3. CDA measures the charge and the mass of an impacting particle, assuming a composition of ice; this can be used to calculate the surface potential (from Kempf et al. 2006). (**b**) Model calculation of the equilibrium surface potential (measured in Volts) of circum-Saturnian grains using a magnetospheric plasma model based on *Voyager* measurements (from Juhász et al. 2002)

grains were positively charged. The electrostatic potential of the grains, detected between 3.5 R_S (212,000 km) and 4.4 R_S (267,000 km), was about –1.6 V, which is consistent with the spacecraft potential measured by the RPWS Langmuir probe (Wahlund et al. 2005), but inconsistent with model calculations using the Voyager model for the Saturnian plasma environment (Richardson 1995, Juhász et al. 2007) which predicts much higher potentials (–5 V). Most likely this results from *Cassini*'s ability to extend electron measurements towards lower energies than the *Voyagers* could. However, the models correctly predict the switch from negative to positive surface potentials to occur in the region between the moons Dione and Rhea; this happens mainly because secondary and photoelectron emissions become increasingly important in this region.

The motion of small grains around a planet can be surprisingly complex due to the competing effects of gravity, drag, radiation pressure, and electromagnetic forces. We now discuss Saturn's E ring as an example where relatively straightforward orbital calculations following the short-term dynamics of particles ejected from Enceladus are capable of elucidating many observations. Since *Cassini*'s discovery of the plumes leaving Enceladus's south polar regions, it seems that the dust production from these geysers is sufficient to sustain the E ring and to fill the entire magnetosphere with grains far beyond the classical boundaries of this ring (Srama et al. 2006).

Dust particles gain an electric charge in Saturn's plasma environment (Fig. 16.15). The orbital regression caused by the corresponding electromagnetic forces for particles with $s \sim 1\,\mu m$ can compensate for the orbital precession due to Saturn's oblateness (see the equation immediately below). This allows the solar radiation pressure to induce large orbital eccentricities for micron-sized particles, spreading them over a broad radial span. Grains much larger or smaller than about a micron remain closer to Enceladus and re-impact the satellite in a short time (Horányi et al. 1992, Hamilton and Burns 1994). With escape speeds $\ll$ orbital speed of Enceladus, the predicted dust distribution in the E ring extends from ~2 to ~7 R_S in the radial direction with the vertical thickness increasing from ~1,000 to ~5,000 km. However, the calculated normal optical depth remained symmetric relative to Enceladus, contrary to observations.

The semi-major axes of dust grains originating from Enceladus will secularly increase once plasma drag is incorporated in the dynamics (Dikarev and Krivov 1998). Such evolution can explain the observed asymmetry in the dust distribution inside and outside Enceladus's orbit. In addition, particle erosion due to sputtering can be surprisingly fast, limiting the lifetime of micron-sized particles to ~50 years in the E ring (Jurac et al. 2001). Detailed dynamical models involve the simultaneous integration of three coupled nonlinear differential equations: (a) the equation of motion that includes gravity, radiation pressure, plasma and neutral drags, and the Lorentz force, calculated assuming a model of the magnetospheric fields and plasmas; (b) the current balance equation to follow a grain's time-dependent charge, including several currents (collection of electrons and ions, secondary and photoelectron production), assuming some material properties for the grains; and (c) the equation describing the mass-loss rate of a grain due to sputtering. These equations involve assumptions about the material properties of the grains, including their density, light-scattering efficiency, and yields of photoelectrons, secondary electrons, and sputtering.

Two *Cassini* discoveries – the active dust-producing geysers in Enceladus's south-polar regions and the E-ring's large radial span, reaching even Titan's orbit – indicate that Enceladus may be dominantly responsible for filling Saturn's entire magnetosphere with dust. Particles are transported outwards from Enceladus due to plasma drag (Morfill et al. 1983, Havnes et al. 1992, Dikarev 1999), but along the way they lose mass via sputtering (Jurac et al. 2001, Burns et al. 2001). These processes compete to eventually determine those regions that particles with a given initial size can reach (Horányi et al. 2008). Plasma drag acting alone produces a slow adiabatic increase in semi-major axis, while radiation pressure induces periodic changes in the orbital eccentricity of a particle, with a period $P = 2\pi/\left(\dot{\varpi}\right)$, and amplitude $A \sim 1/\left(\dot{\varpi}\right)$, where $\dot{\varpi}$ is the precession rate of the longitude of pericenter. Both the planetary oblateness and the Lorentz force acting on a charged grain cause orbital precession that, for Saturn and for small eccentricity and inclination (e, i << 1), can be written as (Horányi et al. 1992)

$$\dot{\varpi} = 51.4a^{-3.5} + 5.1\frac{\phi^V}{s_\mu}a^{-3}, \tag{16.1}$$

where a is the semi-major axis in units of Saturn's radius, ϕ^V is the grain's surface potential in Volts, and s_μ is the dust-particle's radius in μ m. In regions where the plasma environment sets $\phi^V < 0$ (Fig. 16.15), the terms could cancel each other. The outward-drifting and eroding grains can temporarily experience 'locking' $\left(\dot{\varpi} \sim 0\right)$, at which point they swiftly develop large eccentricities. The out-of-plane component of radiation pressure will simultaneously force particles onto inclined orbits (Hamilton 1993, Burns et al. 2001). While this effect remains modest for negatively charged grains, it can be quite significant in regions of positive grain charges, which become destabilized against vertical oscillations (Howard et al. 1999). Additionally, the time-dependent charge of the grains on elliptical orbits moving along and against the co-rotational electric field can lead to swift gains or losses in orbital energy (Burns and Schaffer 1989), while the magnetic-field interaction can result in rapid changes in a particle's orbital angular momentum (Horányi 1996).

Computer simulations following the evolution of the charge, mass, and the orbit of particles escaping from Enceladus's geysers reproduce many E-ring characteristics that have been observed in-situ and remotely, including the spatial and size distributions of the particles comprising the ring, on both large scales and also near the source moon itself (Figs. 16.16 and 16.17). Particles transported from Enceladus to 20 R_S arrive there in about 300 years, but meanwhile have shrunk to only a few percent of their original radii due to sputtering losses. If grains with $s \gg \mu m$ are found at this distance, they would have to be born at one of the more distant moons. However, to date, no dust-density enhancements have been noticed while crossing the ring plane near the orbits of any other satellites. Nonetheless, since small grains have been detected far from Saturn, these calculations therefore indicate that the geysers on Enceladus have been supplying the E-ring material at an approximately constant rate at least for the last 300 years.

16.3.9 Dust Streams

Figure 16.18 documents the discovery of the high-velocity streams of nanometer-sized dust particles originating from the inner Saturnian system (Kempf et al. 2005a, Hsu et al. 2009). This topic is included here because such particles likely are an end-state for E-ring material, and because the same processes that govern the lives of faint-ring material are active on stream particles. Previously, only the Jovian system was known to eject dust (Grün et al. 1993).

During *Cassini*'s approach to Saturn, the dust detector often registered impact signals, which were most likely caused by particles moving faster than 70 km s^{-1}, the fastest impact speed for which CDA was calibrated at the Heidelberg dust-accelerator facility. Small, positively charged grains within Saturn's magnetosphere can be accelerated to high speeds as a result of the outward-pointing electric field induced by Saturn's co-rotating magnetic field, which has a similar configuration to Jupiter's (Horányi et al. 1993, Hamilton and Burns 1993). Calculating the work done by the co-rotating electric field and the expected charges of the grains, a simple order-of-magnitude relationship can be derived to show that the expected escape velocity is inversely proportional to the size of the particles (Horányi 2000):

$$V_{escape} = \frac{3}{s_\mu} \quad \text{km s}^{-1} \text{ for Jupiter, and}$$

$$V_{escape} = \frac{0.6}{s_\mu} \quad \text{km s}^{-1} \text{ for Saturn,}$$

where s_μ is the grain's radius measured in μm. These expressions assume that Jovian dust particles start at Io, and that Saturn's grains are accelerated outward from Dione's distance, since that is where the grains' charge become positive. The faster speeds at Jupiter result mainly from its stronger magnetic field. Dust grains with sizes $0.001 < s_\mu < 0.01$ are expected to leave Saturn's magnetosphere with a speed in the range of $600\,\text{km s}^{-1} > V_{escape} > 60\,\text{km s}^{-1}$, indicating that the detected particles were a few nm in size.

Both the mass and speed of Saturnian stream particles are outside the calibrated range of the *Cassini* dust detector. However, the amount of plasma generated by the impacts should scale with the particle mass and speed. Particles detected after *Cassini*'s orbit insertion generally produced little impact plasma, which is dynamically compatible with an E ring origin. Interestingly, stream particles detected during the approach phase at distances larger than 500 R_S caused large impact charges, which supports an origin from the outskirts of the A ring (Kempf et al. 2005a). Beyond Saturn's magnetosphere, the dynamics of the stream particles are governed by interactions with the interplanetary magnetic field convected by the solar wind (Hsu et al. 2009). *Cassini* observed a continuous flow of stream particles arriving from directions close to the line-of-sight to Saturn. Both the directionality and the strength of the dust streams changed almost instantaneously whenever the *Cassini* magnetometer sensed 'co-rotating interaction regions' (CIRs), which are characterized by compressed flow of high-speed solar-wind plasma and by enhanced magnetic-field strengths. This coincidence suggests that the periodic impact bursts observed by *Ulysses, Galileo, and Cassini* arise from the speed increase of the dust streams during their CIR traversals (Hamilton and Burns 1993, Kempf et al. 2005a, Krüger et al. 2006a).

Saturnian stream particles were found to be composed predominantly of oxygen, silicon and iron, suggesting that they consist of silicate materials (Kempf et al. 2005b). Because Saturn's main rings as well as the E ring are primarily made of water ice, stream particles are suspected to be the impurities embedded in the icy ring material rather than the bulk composition of the particles themselves. Numerical simulations of the stream-particle propagation showed that the majority of these grains started at distances to Saturn between 7 and 9 R_S and leave Saturn's magnetosphere closely aligned with the ring-plane (Hsu et al. 2009). In this region, ring particles are electromagnetically trapped, while their size decreases slowly due to sputtering by the ambient plasma until their charge–to-mass ratio exceeds the critical value for ejection from the ring region (Beckmann et al. 2009).

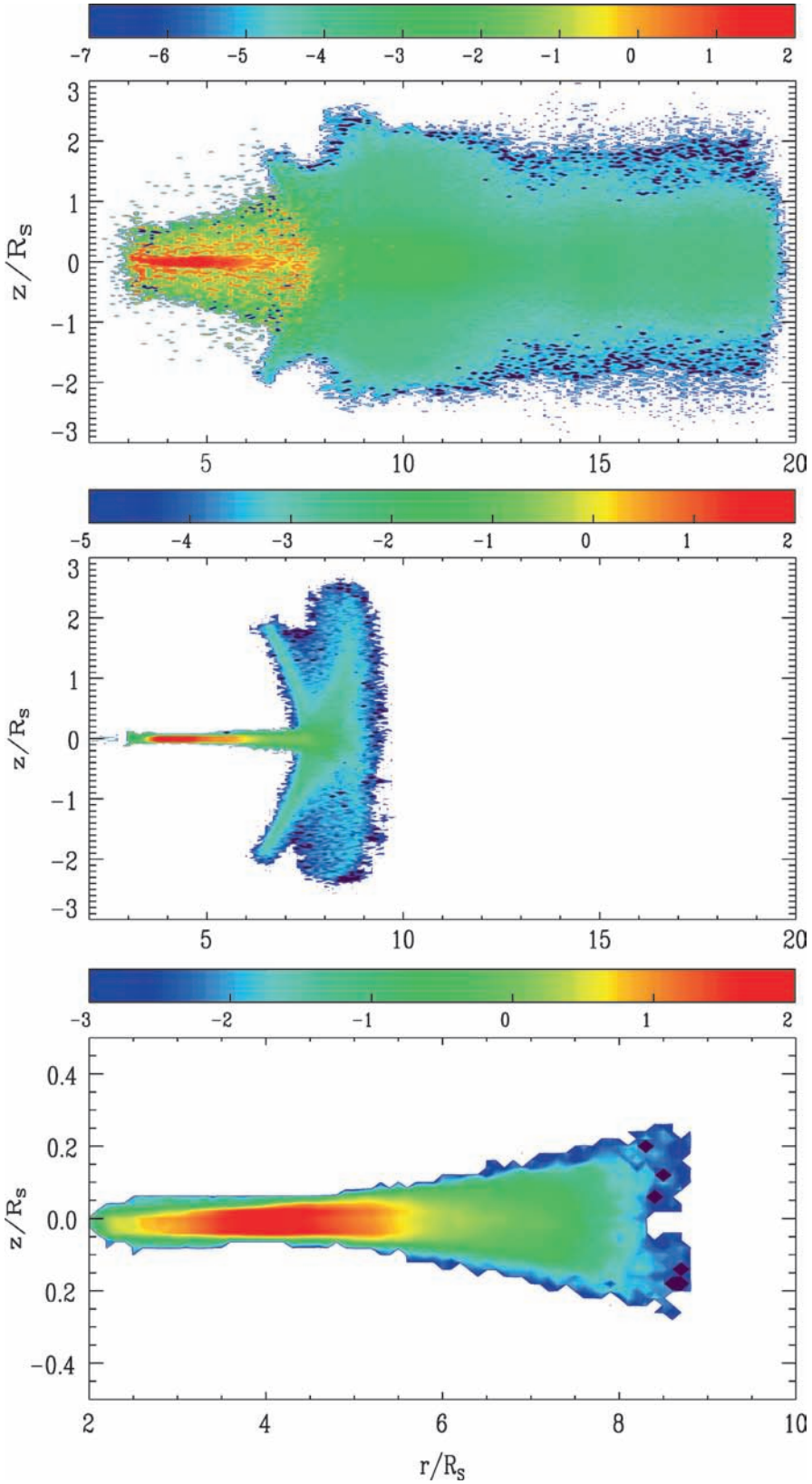

Fig. 16.16 The results of a numerical simulation for the azimuthally averaged density distribution of grains having particular radii: (*top*) 0.1 < s < 0.5 μm; (*middle*) 0.5 < s < 1 μm; and (*bottom*) 1 < s < 3 μm. The largest grains remain confined to the classical E ring, while the smallest particles can reach the orbit of Titan. These simulations started with a power-law size distribution (exponent of –2.5) between 0.1–10 μm with all grains being released from Enceladus with an initial southward velocity of 100 m/s. The color scale is logarithmic, and in each case normalized to 100, corresponding to maximum number densities of 7; 1.2; and 0.3 m^{-3} (from Horányi et al. 2008)

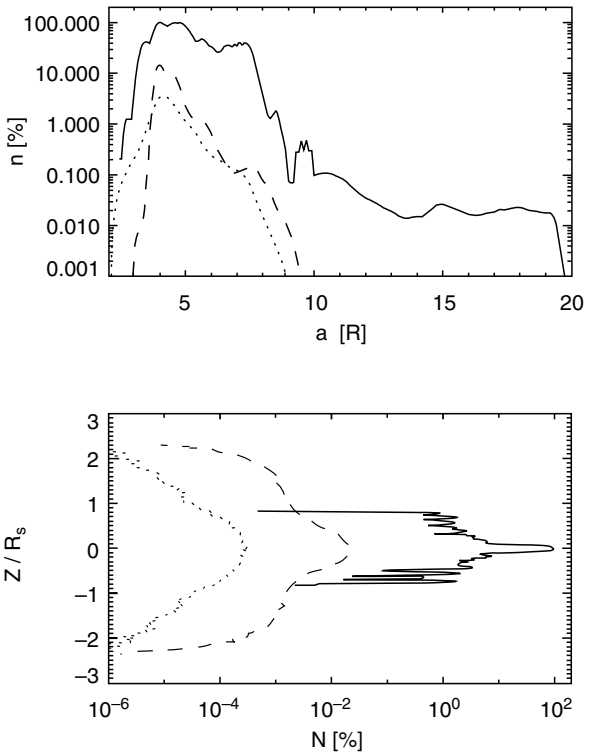

Fig. 16.17 The column densities (*top panel*) as function of distance from Saturn for the same groups of particles as in Fig. 16.16, $0.1 < s < 0.5\,\mu$m (*continuous line*); $0.5\,\mu$m $< s < 1\,\mu$m (*dashed line*); and $1 < s < 3\,\mu$m (*dotted line*). The curves are normalized by setting the maximum density of the smallest grains to 100, corresponding to a real column density of $0.3\,\mathrm{m}^{-2}$. The vertical distribution of the particles (*bottom*) in the size range $0.1 < s < 0.5\,\mu$m, at 5 (*continuous line*); 10 (*dashed line*); and 15 R_S (*dotted line*). The curves are normalized by setting the maximum density at 5 R_S to 100, corresponding to a real number density of $7\,\mathrm{m}^{-3}$ (from Horányi et al., 2008)

16.4 Summary: Dynamical Connections Between Diffuse Rings

The above sections have described various characteristics of individual faint rings and dust populations around Saturn, as well as some attempts that have been made to interpret and model the observed features in specific regions. However, it is important to realize that many of the same physical processes are active in various different dusty rings. In this section we summarize some of the phenomena that appear to be active in several different rings. We maintain that the same ingredients may lead to remarkably different outcomes.

Some of the dust-sized grains observed in the Saturn system are thought to be collisonal debris produced by impacts into, and among, various source bodies close to, or within, the dusty rings (notable exceptions to this being the E ring particles generated by Enceladus's geological activity and the possibly electrostatically levitated grains in the spokes). The Type I particles in the E ring may be generated by impacts of both interplanetary meteoroids and eccentrically orbiting E-ring grains into the surface of the mid-sized satellites like Enceladus. Also, discrete rings are associated with tiny moons (Janus/Epimetheus, Pallene, Methone and Anthe), reminiscent of Jupiter's ring (Burns et al. 1999). A population of larger source bodies has also been identified in the G-ring arc. Comparing the particle properties and size distributions of the material derived from these different sources could clarify how efficiently different-sized source bodies can generate dust grains of various sizes (Burns et al. 1984, 2001).

Several dusty rings show evidence of being influenced by solar radiation. The E-ring's broad expanse could be partly due to periodic changes in the orbital parameters induced

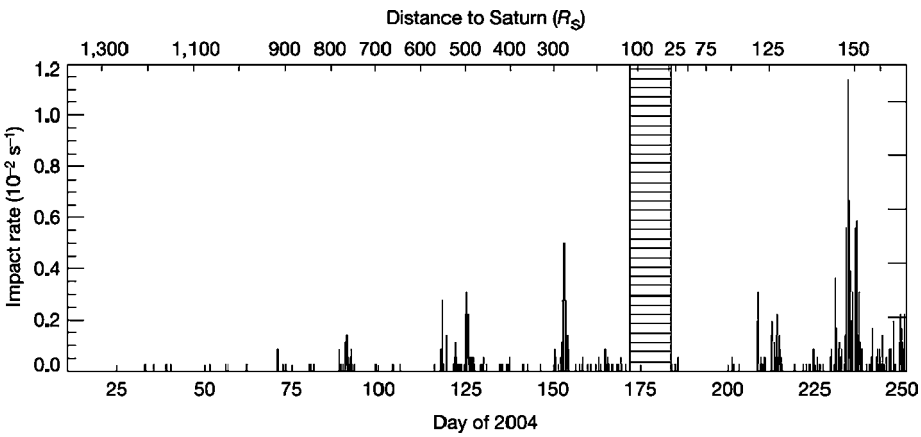

Fig. 16.18 The impact rate registered by the cosmic dust analyzer (CDA) between 10 January and 6 September 2004. During Saturn orbit insertion, marked by horizontal bars, CDA was powered off. The upper scale shows *Cassini*'s distance to Saturn. In total, 1,409 impacts were detected and exhibited the characteristic features of high-velocity impacts by tiny dust particles. Owing to *Cassini*'s changing orientation relative to the arriving particles, the observed flux does not necessarily represent the true temporal variability of the stream particles (from Kempf et al. 2005a)

either by solar radiation pressure (Horányi et al. 1992, Hamilton 1993) or by variations in the particles' charges as they pass through the planet's shadow (Horányi and Burns 1991, Hamilton and Krüger 2008). Meanwhile, some ringlets within the main rings exhibit heliotropic behavior where the entire ringlet seems to be displaced towards the sun. These two systems provide two very different environments in which to explore how solar radiation alters the dynamics of small particles.

Many dusty rings show evidence of being sculpted by resonances with various periodic perturbing forces. Arcs of material confined by co-rotation resonances with Mimas have been found at the orbits of the small moons Anthe and Methone, and in the G ring (Hedman et al. 2007b, 2009a). The outer G ring also contains a structure that appears to be driven by a Lindblad resonance with Mimas. Intriguingly, multiple dust populations in and around the main rings (the middle D ring, inner Roche Division and the spokes in the B ring) reveal periodic structures that appear to be driven by perturbations with characteristic periods between 10.5 and 11 h. This range of periods is close to the periods observed in the SKR and other magnetospheric phenomena, suggesting that all of these regions are being influenced by asymmetries in Saturn's magnetosphere (Burns et al. 1985, Hedman et al. 2009b). Since these dusty systems are qualitatively different from other environments (e.g., dense rings) where resonant phenomena have been extensively studied, detailed modeling of the particle dynamics promise to be very illuminating and may constrain local plasma properties.

Dissipative and drag forces can be observed operating in several different ring systems. The E-ring's broad span almost certainly requires plasma drag to produce secular changes in the semi-major axes of particles launched from Enceladus. The outer flank of the G ring appears to be consistent with particles drifting away from the source bodies in the arc under via interactions with the surrounding plasma. The inner parts of the D ring contain sheets of material that could consist of fine material spirally in towards the planet from various source regions (like the D68 ringlet) due to drag from the planet's upper atmosphere or ionosphere, as has been suggested for the Uranian rings (Colwell and Esposito 1990). Evidence for dissipative processes can also be found in the response of various dusty rings to resonant perturbations. The structures associated with resonances in the G ring, Roche Division and D ring all appear to require some additional physics to dissipate eccentricities on short timescales (10–100 days). Comparisons of the orbital evolution and damping timescales at these various locations should clarify the nature and strength of various sources of dissipation (Hedman et al. 2009b).

Diffuse planetary rings are an excellent laboratory to study dusty plasma processes acting on large scales. Imaging observations, when combined with in-situ measurements of the dust and of the plasma parameters, including the electric and magnetic fields, provide a rich complementary data set. The extension of *Cassini* beyond its prime mission period of 2004–2008 for four more years provides an unprecedented series of observations that cover a full period of Saturnian seasons. To understand the role of the UV radiation due to solar-cycle variability, and to enable the comparison of the diffuse rings and the spokes in the B-ring to their state during the *Voyager* encounters, *Cassini* must remain healthy into 2016 and beyond.

Acknowledgements All authors appreciate the efforts of *Cassini*'s engineers in providing an exceptional mission. MH thanks Antal Juhász for years of fruitful collaboration. JAB recognizes the contributions of numerous former graduate students on ethereal ring problems. JAB, MH and MMH have received support from NASA, the *Cassini-Huygens* Project and CDAP. GHJ holds an STFC Advanced Fellowship. SK acknowledges support from DLR.

References

Akalin, F., Gurnett, D.A., Averkamp, T.F., Persoon, A.M., Santolik, O., Kurth, W.S., Hospodarsky, G.B.: First whistler observed in the magnetosphere of Saturn. Geophys. Res. Ltrs. **33**, L20107 (2006), doi:10.1029/2006GL027019

Aubier, M.G., Meyer-Vernet, N., Pedersen, B.M.: Shot noise from grain and particle impacts in Saturn's ring plane. Geophys. Res. Ltrs. **10**, 5–8 (1983).

Bauer, J., Lissauer, J.J., Simon, M.: Edge-on observations of Saturn's E and G rings in the near-IR. Icarus **125**, 440–445 (1997).

Baum, W. A., Kreidl, T., Westphal, J. A., Danielson, G. E., Seidelmann, P. K., Pascu, D., Currie, D. G.: Saturn's E ring. Icarus **47**, 84–96 (1981).

Beckmann, U., Kempf, S., Spahn, F.: Long-term evolution of Saturn's E ring particles, Icarus, submitted (2009).

Bosh, A.S., Olkin, C.B.: Low optical depth features in Saturn's rings: The occultation of GSC5249–01240 by Saturn and its rings. Bull. Am. Astron. Soc. **28**, 1124 (1996).

Burns, J.A., Schaffer, L.: Orbital evolution of circumplanetary dust by resonant charge variations. Nature **37**, 340–343 (1989).

Burns, J.A., Showalter, M.R., Cuzzi, J.N., Durisen, R.H.: Saturn's electrostatic discharges – Could lightning be the cause? Icarus **54**, 280–295 (1983).

Burns, J.A., Showalter, M.R., Morfill, G.E.: The ethereal rings of Jupiter and Saturn. In: Greenberg, R., Brahic, A. (eds.) *Planetary Rings*, pp. 200–274. Univ. Ariz. Press, Tucson (1984).

Burns, J.A., Schaffer, L., Greenberg, R.J., Showalter, M.R.: Lorentz resonances and the structure of the Jovian ring. Nature **316**, 115–119 (1985).

Burns, J.A., Showalter, M.R., Hamilton, D.P., Nicholson, P.D, de Pater, I., Ockert-Bell, M., Thomas, P.C.: The formation of Jupiter's faint rings. Science **284**, 1146–1150 (1999).

Burns, J.A., Hamilton, D.P., Showalter, M.R.: Dusty rings and circumplanetary dust: Observations and simple physics. In: Grün, E., Gustafson, B., Dermott, S., Fectig, H. (eds.) Interplanetary Dust, pp. 641–725. Springer, Berlin (2001).

Burns, J.A., Hedman, M.M., Tiscareno, M.S., Nicholson, P.D., Streetman, B.J., Colwell, J.E., Showalter, M.R., Murray, C.D., Cuzzi, J.N., Porco, C.C., ISS Team: Morphology, movements and models

of ringlets in Saturn's Encke Gap. Bull. Am. Astro. Soc. **37**, 766 (2005).

Burt, J.A., Hedman, M.M., Tiscareno, M.S., Burns, J.A.: The where and why of Saturn's inclined "Charming" ringlet. Bull. Am. Astro. Soc. **40**, 445 (2008).

Colwell, J.E., Esposito, L.W.: A numerical model of the Uranian dust rings. Icarus **86**, 530–560 (1990).

Cooper, N.J., Murray, C.D., Evans, M.W., Beurle, K., Jacobson, R.A., Porco, C.C.: Astrometry and dynamics of Anthe (S/2007S4), a new satellite of Saturn. Icarus **195**, 765–777 (2008).

Cuzzi, J.N., Durisen, R.H.: Bombardment of planetary rings by meteoroids – General formulation and effects of Oort Cloud projectiles. Icarus **84**, 467–501 (1990).

de Pater, I., Showalter, M.R., Lissauer, J.J., Graham, J.R.: Keck infrared observations of Saturn's E and G rings during Earth's 1995 ring plane crossings. Icarus **121**, 195–198 (1996).

de Pater, I., Martin, S.C., Showalter, M.R.: Keck near-infrared observations of Saturn's E and G rings during Earth's ring-plane crossing in August 1995. Icarus **172**, 446–454 (2004).

Dikarev, V.V.: Dynamics of particles in Saturn's E ring: Effects of charge variations and the plasma drag force. Astron. Astrophys. **346**, 1011–1019 (1999).

Dikarev V.V., Krivov, A.V.: Dynamics and spatial distribution of particles in Saturn's E ring. Solar Sys. Res. **32**, 128 (1998).

Doyle, L.R., Grün, E.: Radiative transfer modeling constraints on the size of the spoke particles in Saturn's rings. Icarus **85**, 168–190 (1990).

Eplee, R.E., Smith, B.A.: Spokes in Saturn's rings – Dynamical and reflectance properties. Icarus **59**, 188–198 (1984).

Farmer, A.J., Goldreich, P.: Spoke formation under moving plasma clouds. Icarus **179**, 535–538 (2005).

Farrell, W.M., Desch, M.D., Kaiser, M.L., Kurth, W.S., Gurnett, D.A.: Changing electrical nature of Saturn's rings: Implications for spoke formation, Geophys. Res. Ltrs., **33**, L07203(2006). doi:10.1029/2005GL024922

Feibelman, W.: Concerning the "D" ring of Saturn. Nature **214**, 793–794 (1967).

Ferrari, C., Brahic, A.: Arcs and clumps in the Encke division of Saturn's rings. Planet. Space Sci. **45**, 1051–1067 (1997).

Fischer, G., Desch, M.D., Zarka, P., Kaiser, M.L., Gurnett, D.A., Kurth, W.S., Macher, W., Rucker, H.O., Lecacheux, A., Farrell, W.M., Cecconi, B.: Saturn lightning recorded by *Cassini* RPWS in 2004. Icarus **183**, 135–152 (2006).

Goertz, C.K., Morfill, G.: A model for the formation of spokes in Saturn's rings. Icarus **53**, 219–229 (1983).

Gresh, D.L., Rosen, P.A., Tyler, G.L., Lissauer, J.J.: An analysis of bending waves in Saturn's rings using *Voyager* radio occultation data. Icarus **68**, 481–502 (1986).

Grün, E., Morfill, G.E., Terrile, R.J., Johnson, T.V., Schwehm, G.: The evolution of spokes in Saturn's B ring. Icarus **54**, 227–252 (1983).

Grün, E., Morfill, G.E., Mendis, D.A.: Dust-magnetosphere interactions. In: Greenberg, R., Brahic, A. (eds.) *Planetary Rings*, pp. 275–332. Univ. Ariz. Press, Tucson (1984).

Grün, E., Goertz, C.K., Morfill, G. E., Havnes, O.: Statistics of Saturn's spokes. Icarus **99**, 191–201 (1992).

Grün, E., Zook, H., Baguhl, M., Balogh, A., Bame, S., Fechtig, H., Forsyth, R., Hanner, M., Horányi, M., Kissel, J., Lindblad, B.-A., Linkert, D., Linkert, G., Mann, I., McDonnell, J.A.M., Morfill, G., Phillips, J., Polanskey, C., Schwehm, G., Siddique, N., Staubach, P., Svestka, J., Taylor, A.: Discovery of Jovian dust streams and interstellar grains by the *Ulysses* spacecraft. Nature **362**, 428–430 (1993).

Gurnett, D.A., Grün, E., Gallagher, D., Kurth, W.S., Scarf, F.L.: Micron-sized particles detected near Saturn by the *Voyager* plasma wave instrument. Icarus **53**, 236–254 (1983).

Gurnett, D.A., Kurth, W.S., Wang, Z., Persoon, A.M., Groene, J.B., Averkamp, T.F., Zarka,P., Farrell, W.M., Kaiser, M.L.: An overview of the rotational modulation of three types of Saturnian radio emissions. AGU Fall Meeting P23C-07 (2007).

Hamilton, D.P.: Motion of dust in a planetary magnetosphere: Orbit-averaged equations for oblateness, electromagnetic and radiation forces with application to Saturn's E ring. Icarus **101**, 244–264 (1993).

Hamilton, D.P.: A comparison of Lorentz, gravitational, and satellite gravitational resonances. Icarus **109**, 221–240 (1994).

Hamilton, D.P.: The collisional cascade model for Saturn's ring spokes. Bull. Am. Astron. Soc. **38**, 578 (2006).

Hamilton, D.P., Burns, J.A.: Ejection of dust from Jupiter's gossamer ring. Nature **364**, 695–699 (1993).

Hamilton, D.P., Burns, J.A.: Origin of Saturn's E ring: Self-sustained, naturally. Science **264**, 550–553 (1994).

Hamilton, D.P., Krüger, H.: The sculpting of Jupiter's gossamer rings by its shadow. Nature **453**, 72–75 (2008).

Havnes, O., Morfill, G.E., Melandso, F.: Effects of electromagnetic and plasma drag forces on the orbital evolution of dust in planetary magnetospheres. Icarus **98**, 141–150 (1992).

Hedman, M.M., Burns, J.A., Showalter, M.R., Porco, C.C., Nicholson, P.D., Bosh, A.S., Tiscareno, M.S., Brown, R.H., Buratti, B.J., Baines, K.H., Clark, R.: Saturn's dynamic D ring. Icarus **188**, 89–107 (2007a).

Hedman, M.M., Burns, J.A., Tiscareno, M.S., Porco, C.C., Jones, G.H., Roussos, E., Krupp, N., Paranicas, C., Kempf, S.: The source of Saturn's G ring. Science **317**, 653–656 (2007b).

Hedman, M.M., Burns, J.A., Tiscareno, M.S., Porco, C.C.: The heliotropic rings of Saturn. Bull. Am. Astron. Soc. **39**, 427 (2007c).

Hedman, M.M., Murray, C.D., Cooper, N.J., Tiscareno, M.S., Beurle, K., Evans, M.W., Burns, J.A.: Three tenuous rings/arcs for three tiny moons. Icarus **199**, 378–386 (2009a).

Hedman, M.M., Burns, J.A., Tiscareno, M.S., Nicholson, P.D., Porco, C.C.: Organizing some very tenuous things: Resonant structures in Saturn's faint rings. Icarus **202**, 260–279 (2009b). doi: 10.1016/j.icarus.2009.02.016

Hedman, M.M., Nicholson, P.D., Showalter, M.R., Brown, R.H., Buratti, B.J., Clark, R.N.: Spectral observations of the Enceladus plume with *Cassini* VIMS. Astrophys. J. **693**, 1749–1762 (2009c).

Hill, J.R., Mendis, D.A.: On the braids and spokes in Saturn's ring system, Moon Planets **24**, 431–436 (1981).

Hill, J.R., Mendis, D.A.: The dynamical evolution of the Saturn ring spokes. J. Geophys. Res. **87**, 7413–7420 (1982).

Hillier, J.K., Green, S.F., McBride, N., Schwanethal, J.P., Postberg, F., Srama, R., Kempf, S., Moragas-Klostermeyer, G., McDonnell, J.A.M., Grün, E.: The composition of Saturn's E ring. MNRAS **377**, 1588–1596 (2007).

Horányi, M.: Charged dust dynamics in the solar system. Ann. Rev. Astron. Astrophys. **34**, 383–418 (1996).

Horányi, M.: Dust streams from Jupiter and Saturn. Phys. Plasmas **7**, 3847–3850 (2000).

Horányi, M., Burns, J.A.: Charged-dust dynamics – Orbital resonance due to planetary shadows. J. Geophys. Res. **96**, 19,283–19,289 (1991).

Horányi, M., Burns, J.A., Hamilton, D.P.: The dynamics of Saturn's E ring particles. Icarus **97**, 248–259 (1992).

Horányi, M., Morfill, G., Grün, E.: Mechanism for the acceleration and ejection of dust grains from Jupiter's magnetosphere. Nature **363**, 144–146 (1993).

Horányi, M., Hartquist, T.W., Havnes, O., Mendis, D.A., Morfill, G.E.: Dusty plasma effects in Saturn's magnetosphere. Rev. Geophys. **42** (2004) RG4002. doi: 10:1029/2004 RG000151

Horányi, M., Juhász, A., Morfill, G.: The large scale structure of Saturn's E ring, Geophys. Res. Ltrs. **35**, L04203 (2008). doi: 10.1029/2007GL032726

Howard, J.E., Horányi, M., Stewart, G.R.: Global dynamics of charged dust grains in planetary magnetospheres. Phys. Rev. Ltrs. **83**, 3993–3996 (1999)

Hsu, H.-W., Kempf, S., Jackman, C.M.: Observations of Saturnian stream particles in the interplanetary space. Icarus, in press (2009).

Juhász, A., Horányi, M.: Saturn's E ring: A dynamical approach. Jnl. Geophys. Res. **107** (2002). doi: 10.1029/2001JA 000182

Juhász, A., Horányi, M., Morfill, G. E.: Signatures of the Enceladus plumes in Saturn's E-ring. Geophys. Res. Ltrs. **34**, L09104 (2007). doi: 10.1029/2006 GL 029120

Jones, G. H., Krupp, N., Krüger, H., Roussos, E., Ip, W.-H., Mitchell, D. G., Krimigis, S. M., Woch, J., Lagg, A., Fränz, M., Dougherty, M. K., Arridge, C. S., McAndrews, H. J.: Formation of Saturn's ring spokes by lightning-induced electron beams. Geophys. Res. Ltrs. **33**, L21202 (2006). doi:10.1029/2006GL028146

Jurac, S., Johnson, R.E., Richardson, J.D., Paranicas, C.: Satellite sputtering in Saturn's magnetosphere. Planet. Space Sci. **49**, 319–326 (2001).

Kempf, S., Srama, R., Horányi, M., Burton, M., Helfert, S., Moragas-Klostermeyer, G., Roy, M., Grün, E.: High-velocity streams of dust originating from Saturn. Nature **433**, 289–291 (2005a).

Kempf, S., Srama, R., Postberg, F., Burton, M., Green, S. F., Helfert, S., Hillier, J. K., McBride, N., McDonnell, J. A. M., Moragas-Klostermeyer, G., Roy, M., Grün, E.: Composition of Saturnian stream particles. Science **307**, 1274–1276 (2005b).

Kempf, S., Beckmann, U., Srama, R., Horányi, M., Auer, S., Grün, E.: The electrostatic potential of E ring particles. Planet. Space Sci. **54**, 999–1006 (2006).

Kempf, S., Beckmann, U., Moragas-Klostermeyer, G., Postberg, F., Srama, R., Economou, T., Schmidt, J., Spahn, F., Grün, E.: The E ring in the vicinity of Enceladus. I: Spatial distribution and properties of the ring particles. Icarus **193**, 420–437 (2008).

Kempf, S., Beckmann, U., Schmidt, J.: Icarus, submitted (2009).

Krimigis, S.M., Mitchell, D.G., Hamilton, D.C., Livi, S., Dandouras, J., Jaskulek, S., Armstrong, T.P., Boldt, J.D., Cheng, A.F., Gloeckler, G., Hayes, J.R., Hsieh, K.C., Ip, W.-H., Keath, E.P., Kirsch, E., Krupp, N., Lanzerotti, L.J., Lundgren, R., Mauk, B.H., McEntire, R.W., Roelof, E.C., Schlemm, C.E., Tossman, B.E., Wilken, B., Williams, D.J.: Magnetosphere Imaging Instrument (MIMI) on the *Cassini* Mission to Saturn/Titan. Space Sci. Rev. **114**, 223–329 (2004).

Krivov, A.V., Sremčević, M., Spahn, F., Dikarev, V.V., Kholshevnikov, K.V.: Impact-generated clouds around planetary satellites: Spherically symmetric case. Planet. Space Sci. **51**, 251–269 (2003).

Krüger, H., Graps, A., Hamilton, D. P., Flandes, A., Forsyth, R.J., Horányi, M., Grün, E.: *Ulysses* jovian latitude scan of high-velocity dust streams originating from the jovian system. Planet. Space Sci. **54**, 919–931 (2006a).

Krüger, H., Altobelli, N., Andweiler, B., Dermott, S.F., Dikarev, V.V., Graps, A.L., Grün, E., Gustafson, B.A.: Five years of *Ulysses* dust data: 2000–2004. Planet. Space Sci. **54**, 932–956 (2006b).

Kurth, W.S., Averkamp, T.F., Gurnett, D.A., Wang, Z.: *Cassini* RPWS observations of dust in Saturn's E Ring. Planet. Space Sci. **54**, 988–998 (2006).

Kurth, W.S., Lecacheux, A., Averkamp, T.F., Groene, J.B., Gurnett, D.A.: A Saturnian longitude system based on a variable kilometric radiation period. Geophys. Res. Ltrs. **34**, L02201 (2007).

Lehtinen, N.G., Inan, U.S., Bell, T.F.: Trapped energetic electron curtains produced by thunderstorm-driven relativistic runaway electrons. Geophys. Res. Ltrs. **27**, 8, 1095–1098 (2000).

Lissauer, J.J., French, R.G.: HST high-resolution backscatter image of Saturn's G ring. Icarus **146**, 12–18 (2000).

Marley, M., Porco, C.C.: Planetary acoustic mode seismology – Saturn's rings. Icarus **106**, 508–524 (1993).

McGhee, C.A., French, R.G., Dones, L., Cuzzi, J.N., Salo, H.J., Danos, R.: HST observations of spokes in Saturn's B ring. Icarus **173**, 508–521 (2005).

Mendis, D.A., Hill, J.R., Ip, W.-H., Goertz, C.K., Grün, E.: Electrodynamic processes in the ring system of Saturn. In: Gehrels, T. (ed.) *Saturn*, pp. 546–589. Univ. Ariz. Press, Tucson (1984).

Meyer-Vernet, N., Lecacheux, A., Pedersen, B. M.: Constraints on Saturn's E ring from the *Voyager* 1 radio astronomy instrument. Icarus **123**, 113–128 (1996).

Mitchell, C.J., Horányi, M., Havnes, O., Porco, C.C.: Saturn's spokes: Lost and found. Science **311**, 1587–1589 (2006).

Mitchell, C.J., Porco, C., Dones, L., Spitale, J.: Analysis of the behavior of spokes in Saturn's B ring as observed in *Cassini* ISS images. Bull. Am Astro. Soc. **40**, 429 (2008).

Moore, L. E., Mendillo, M., Müller-Wodarg, I. C. F., Murr, D. L.: Modeling of global variations and ring shadowing in Saturn's ionosphere. Icarus **172**, 503–520 (2004).

Morfill, G. E., Grün, E., Johnson, T.V.: Saturns's E, G and F rings – Modulated by the plasma sheet? Jnl. Geophys. Res. **88**, 5573–5579 (1983).

Morfill, G.E., Thomas, H.M.: Spoke formation under moving plasma clouds – The Goertz-Morfill model revisited. Icarus **179**, 539–542 (2005).

Nicholson, P.D., Showalter, M.R., Dones, L., French, R.G., Larson, S.M., Lissauer, J.J., McGhee, C.A., Seitzer, P., Sicardy, B., Danielson, G.E.: Observations of Saturn's ring-plane crossing in August and November 1995. Science **272**, 509–515 (1996).

Ockert-Bell, M.E., Burns, J.A., Daubar, I.J., Thomas, P.C., Veverka, J., Belton, M.J.S., Klaasen, K.P.: The structure of Jupiter's ring system as revealed by the *Galileo* imaging experiment. Icarus **138**, 188–213 (1999).

Porco, C. C.: *Voyager* observations of Saturn's rings. 1. The eccentric rings at 1.29, 1.45, 1.95 and 2.27 R_s. 2. The periodic variation of spokes. PhD thesis, California Institute of Technology, Pasadena, CA (1983).

Porco, C.C. on behalf of *Cassini* ISS team: Rings of Saturn (R/2006S1, R/2006S2, R/2006S3, R/2006S4). IAU Circ. **8759** 1 (2006).

Porco, C.C. on behalf of *Cassini* ISS team: S/2008 S1. IAU Circ. **9023** 1 (2009).

Porco, C.C., Danielson, G.E.: The periodic variation of spokes in Saturn's rings. Astron. J. **87**, 826–833 (1982).

Porco, C.C., Baker, E., Barbara, J., Beurle, K., Brahic, A., Burns, J.A., Charnoz, S., Cooper, N., Dawson, D.D., Del Genio, A.D., Denk, T., Dones, L., Dyudina, U., Evans, M.W., Giese, B., Grazier, K., Helfenstein, P., Ingersoll, A.P., Jacobson, R.A., Johnson, T.V., McEwen, A., Murray, C.D., Neukum, G., Owen, W.M., Perry, J., Roatsch, T., Spitale, J., Squyres, S., Thomas, P., Tiscareno, M., Turtle, E., Vasavada, A.R., Veverka, J., Wagner, R., West, R.: *Cassini* imaging science: Initial results on Saturn's rings and small satellites. Science **307**, 1226–1236 (2004).

Porco, C.C., Helfenstein, P., Thomas, P.C., Ingersoll, A.P., Wisdom, J., West, R., Neukum, G., Denk, T., Wagner, R., Roatsch, T., Kieffer, S., Turtle, E., McEwen, A., Johnson, T.V., Rathbun, J., Veverka, J., Wilson, D., Perry, J., Spitale, J., Brahic, A., Burns, J.A., Del Genio, A.D., Dones, L., Murray, C.D., Squyres, S.: *Cassini* observes the active South Pole of Enceladus. Science **311**, 1393–1401 (2005).

Postberg, F., Kempf, S., Hillier, J. K., Srama, R., Green, S. F., McBride, N., Grün, E.: The E-ring in the vicinity of Enceladus II: Signatures of Enceladus in the elemental composition of E-ring particles. Icarus **193**, 438–454 (2008).

Postberg, F., Kempf, S., Brilliantov, N., Schmidt, J., Buck, U., Srama, R.: Sodium in E ring particles implies ocean below the Enceladus' surface. Nature **459**(7250), 1098–1101 (2009).

Richardson, J.: An extended plasma model for Saturn. Geophys. Res. Lett. **22**, 1177–1180 (1995).

Robinson, L. J.: Closing in on Saturn. Sky Tel. **60**, 481 (1980).

Roddier, C., Roddier, F., Graves, J.E., Northcott, M.J.: Discovery of an arc of particles near Enceladus' orbit: A possible key to the origin of the E ring. Icarus **136**, 50–59 (1998).

Roussos, E., Jones, G.H., Krupp, N., Paranicas, C., Mitchell, D.G., Lagg, A., Woch, J., Motschmann, U., Krimigis, S.M., Dougherty, M.K.: Electron microdiffusion in the Saturnian radiation belts: *Cassini* MIMI/LEMMS observations of energetic electron absorption by the icy moons, J. Geophys. Res. **112**, A06214 (2007).

Roussos, E., Jones, G.H., Krupp, N., Paranicas, C., Mitchell, D.G., Krimigis, S.M., Woch, J., Lagg, A., Khurana, K.: Energetic electron signatures of Saturn's smaller moons: Evidence of an arc of material at Methone. Icarus **193**, 455–464 (2008).

Sanchez-Lavega, A., Rojas, J.F., Sada, P.V.: Saturn's zonal winds at cloud level. Icarus **167**, 405–420 (2000).

Schmidt. J, Sremčević, M.: The shadows of Saturn's icy satellites in the E Ring. Geophys. Res. Ltrs., submitted (2009).

Schmidt, J., Brilliantov, N., Spahn, F., Kempf, S.: Slow dust in Enceladus's plume from condensation and wall collisions in tiger stripe fractures. Nature **451**, 685–688 (2008).

Showalter, M.R.: Saturn's D ring in the *Voyager* images. Icarus **124**, 677–689 (1996).

Showalter, M.R., Cuzzi, J.N.: Seeing ghosts: Photometry of Saturn's G ring. Icarus **103**, 124–143 (1993).

Showalter, M.R., Cuzzi, J.N., Larson, S.M.: Structure and particle properties of Saturn's E ring. Icarus **94**, 451–473 (1991).

Showalter, M.R., Hamilton, D.P., Burns, J.A., de Pater, I., Simonelli, D.P.: Structure of Jupiter's main ring and halo from *Galileo* SSI and Earth-based images. In: Bagenal, F. (ed.) *Conference* "*Jupiter: Planet, Satellites and Magnetosphere*," pp. 101–102. LASP, Boulder (2001).

Smith, B.A., Soderblom, L., Beebe, R.F., Boyce, J., Briggs, G., Bunker, A., Collins, S.A. Hansen, C.J., Johnson, T.V., Mitchell, J.L., Terrile, R.J., Carr, M.H., Cook, A.F., Cuzzi, J.N., Pollack, J.B., Danielson, G.E., Ingersoll, A.P., Davies, M.E., Hunt, G.E., Masursky, H., Shoemaker, E.M., Morrison, D., Owen, T., Sagan, C., Veverka, J., Strom, R., Suomi, V.E.: Encounter with Saturn – *Voyager 1* imaging science results. Science **212**, 163–191 (1981).

Smith, B.A., Soderblom, L., Batson, R., Bridges, P., Inge, J., Masursky, H., Shoemaker, E., Beebe, R., Boyce, J., Briggs, G., Bunker, A., Collins, S.A., Hansen, C.J., Johnson, T.V., Mitchell, J.L., Terrile, R.J., Cook, A.F., Cuzzi, J., Pollack, J.B., Danielson, G.E., Ingersoll, A., Davies, M.E., Hunt, G.E., Morrison, D., Owen, T., Sagan, C., Veverka, J., Strom, R., Suomi, V.E.: A new look at the Saturn system: The *Voyager 2* images. Science **215**, 505–537 (1982).

Spahn, F., Schmidt, J., Albers, N., Hörning, M., Makuch, M., Seiß, M., Kempf, S., Srama, R., Dikarev, V., Helfert, S., Moragas-Klostermeyer, G., Krivov, A.V., Sremčević, M., Tuzzolino, A.J., Economou, T., Grün, E.: *Cassini* dust measurements at Enceladus and implications for the origin of the E ring. Science **311**, 1416–1418 (2006).

Spencer, J., Pearl, J.C., Segura, M., Flasar, F.M., Manoutkine, A., Romani, P., Buratti, B.J., Hendrix, A.R., Spilker, L.J., Lopes, R.M.C.: *Cassini* encounters Enceladus: Background and the discovery of a south-polar hot spot. Science **311**, 1401–1405 (2006).

Spitale, J.N., Porco, C.C.: Association of the jets of Enceladus with the warmest regions on its south-polar fractures. Nature **449**, 695–699 (2007).

Spitale, J.N., Jacobson, R.A., Porco, C.C., Owen, W.M.: The orbits of Saturn' small satellites derived from combined historic and *Cassini* Imaging observations. Astron. J. **132**, 692–710 (2006).

Srama, R., Ahrens, T.J., Altobelli, N., Auer, S., Bradley, J.G., Burton, M., Dikarev, V.V., Economou, T., Fechtig, H., Görlich, M., Grande, M., Graps, A., Green, S.F., Grande, M., Grün, E., Havnes, O., Helfert, S., Hillier, J.K., Horányi, M., Igenbergs, E., Jessberger, E.K., Johnson, T.V., Kempf, S., Krivov, A.V., Krüger, H., Mocher-Ahlreep, A., Morgas-Klostermeyer, G., Lamy, P., Landgraf, M., Linkert, D., Linkert, G., Lura, F., McDonnell, J.A.M., Möhlmann, D., Morfill, G.E., Müller, M., Roy, M., Schafer, G., Schlotzhaurer, G., Schwehm, G.H., Spahn, F., Stübig, M., Svestka, J., Tschernjawski, V., Tuzzolino, A.J., Wäsch, R., Zook, H.A.: The *Cassini* Cosmic Dust Analyzer. Space Sci. Rev. **114**, 465–518 (2004).

Srama, R., Kempf, S., Moragas-Klostermeyer, G., Helfert, S., Ahrens, T.J., Altobelli, N., Auer, S., Beckmann, U., Bradley, J.G., Burton, M., Dikarev, V.V., Economou, T., Fechtig, H., Green, S.F., Grande, M., Havnes, O., Hillier, J.K., Horányi, M., Igenbergs, E., Jessberger, E.K., Johnson, T.V., Krüger, H., Matt, G., McBride, N., Mocker, A., Lamy, P., Linkert, D., Linkert, G., Lura, F., McDonnell, J.A.M., Möhlmann, D., Morfill, G.E., Postberg, F., Roy, M., Schwehm, G.H., Spahn, F., Svestka, J., Tschernjawski, V., Tuzzolino, A.J., Wäsch, R., Grün, E.: In-situ dust measurements in the inner Saturnian system. Planet. Space Sci. **54**, 967–987 (2006).

Tagger, M., Henricksen, R.N., Pellat, R.: On the nature of the spokes in Saturn's rings. Icarus **91**, 297–314 (1991).

Thomsen, M.F., Van Allen, J.A.: Motion of trapped electrons and protons in Saturn's inner magnetosphere. J. Geophys. Res. **85**, A11, 5831 – 5834 (1980).

Throop, H.B., Esposito, L.W.: G ring particle sizes derived from ring plane crossing observations. Icarus **131**, 152–166 (1998).

Van Allen, J.: Absorption of energetic protons by Saturn's Ring G. J. Geophys. Res. **88**, A9, 6911–6918 (1983).

Van Allen, J.: An upper limit on the sizes of the shepherd satellites of Saturn's ring G. J. Geophys. Res. **92**, 1153–1159 (1987).

Wahlund, J.E., Boström, R., Gustafsson, G., Gurnett, D.A., Kurth, W.S., Averkamp, T., Hospodarsky, G.B., Persoon, A.M., Canu, P., Pedersen, A., Desch, M.D., Eriksson, A.I., Gill, R., Morooka, M.W., André, M.: The inner magnetosphere of Saturn: *Cassini* RPWS cold plasma results from the first encounter. Geophys. Res. Lett. **32**, L20S09 (2005).

Waite, J. H., Cravens, T. E., Ip, W.-H., Kasprzak, W. T., Luhmann, J. G., McNutt, R. L., Niemann, H. B., Yelle, R. V., Müller-Wodarg, I., Ledvina, S. A., Scherer, S.: Oxygen ions observed near Saturn's A ring. Science **307**, 1260–1262 (2005).

Yaroshenko, V., Horányi, M., Morfill, G.: The wave mechanism of spoke formation in Saturn's rings. In: Multifacets of Dusty Plasmas, Fifth Int'l. Conf. Physics of Dusty Plasmas. AIP Conf. Proc. **1041**, 215–216 (2008).